



# City Research Online

## City St George's, University of London

**Citation:** Liang, S-L., Fu, F., Huang, Z-Q. & Qian, K. (2023). Enhancement of collapse-resistant capacity of non-seismically designed RC frames using various CFRP strengthening schemes. *Engineering Structures*, 291, 116450. doi: 10.1016/j.engstruct.2023.116450

This is the accepted version of the paper.

This version of the publication may differ from the final published version. To cite this item please consult the publisher's version.

**Permanent repository link:** <https://openaccess.city.ac.uk/id/eprint/30716/>

**Link to published version:** <https://doi.org/10.1016/j.engstruct.2023.116450>

**Copyright and Reuse:** Copyright and Moral Rights remain with the author(s) and/or copyright holders. Copies of full items can be used for personal research or study, educational, or not-for-profit purposes without prior permission or charge, unless otherwise indicated, provided that the authors, title and full bibliographic details are credited, a hyperlink and/or URL is given for the original metadata page and the content is not changed in any way. For full details of reuse please refer to [City Research Online policy](#).



29 of beam rebar near the side columns. The strengthening schemes planned to increase the CA capacity or  
30 both the CAA and CA capacities could increase not only the CAA capacity but also the CA capacity. The  
31 enhanced load resistance at the CA stage was mainly attributed to the continuous CFRP strips attached to  
32 the soffits. Unfortunately, the energy method demonstrated that the dynamic load resistance of the tested  
33 sub-frames to prevent collapse was achieved at the CAA stage rather than the CA stage because of the  
34 severe load resistance softening. Thus, the efforts devoted to increasing the CA capacity by this paper  
35 were valid in a real collapse of building scenario. In addition, 113 available test results were collected to  
36 compare with the acceptance criteria in existing codes for collapse-resistant design. Based on the test  
37 results and comparison, design suggestions were given for the collapse-resistant design.

38 **Keywords:** Collapse-resistant; Non-seismically design; Reinforced concrete; CFRP; Strengthening  
39 schemes

40 \*Corresponding author. E-mail address: qiankai@glut.edu.cn

## 41 **1. Introduction**

42 Progressive collapse is defined as “the spread of an initial local failure from element to element,  
43 eventually resulting in the collapse of an entire structure or a disproportionately large part of it”[1]. The  
44 initial local failure of the structural element can be caused by various extreme occasional loads, such as  
45 blast, impact, and fire. However, the state of the art of collapse-resistant design of buildings neglects the  
46 type and intensity of the occasional loads but introduces the “Alternative load path method” by  
47 investigating column removal scenario to assess the performance of the damaged building to bridge the  
48 initial local failure. In this case, the internal forces of the structural elements above the removed column  
49 can be well beyond the design envelope, which necessitates the mobilization of secondary load transfer  
50 mechanisms to resist collapse.

51 To date, extensive tests have been conducted to demonstrate the behavior of reinforced concrete  
52 (RC) frames under the column removal scenario [2-7]. It was found that pure flexural action is always  
53 able to develop at the initial loading stage, and then compressive arch action (CAA) begins to dominate  
54 the load transfer once sufficient axial constraints are applied to the beam ends. Otherwise, only the pure  
55 flexural action can be activated, such as in the case under a corner column removal scenario [8, 9]. The  
56 development of CAA is associated with the beam axial compression force and the CAA capacity is found

57 to be mainly related to concrete compressive strength, longitudinal reinforcement ratio, and span/depth  
58 ratio of the beam. The enhancement ratio of CAA, which is defined as the ratio of CAA capacity to yield  
59 load (YL) capacity, increases nearly linearly with the increase of compressive strength of concrete but  
60 decreases with the increase of mechanical reinforcement ratio, and it is the most sensitive to span/depth  
61 ratio of the beam [5, 7, 10, 11]. After the CAA stage, a transition stage can occur prior to the CA stage,  
62 during which the beam axial compression force begins to convert to axial tension force. The CA can be  
63 activated or not is highly dependent on the rotational capacity of the beam ends and boundary conditions  
64 (performance of side joint and side column), the former affects the development level of CA while the  
65 latter determines the material property of the beam longitudinal rebar can be sufficiently utilized or not.  
66 For example, in FarhangVesali et al. [5] and Vali pour et al. [10]'s tests, the beam tension rebar at both  
67 beam ends of a beam successively fractured at the CAA stage, consequently, the beam rotated freely  
68 because the rotational constraints at the beam ends were released, resulting in a severe load softening  
69 after the CAA stage and subsequent limited development of CA. In addition, shear failure of the side  
70 beam-column joints [3, 12-14] and large eccentric compression failure of the side columns [15-17] can  
71 prevent the sufficient mobilization of CA. It is worthwhile noting that the majority of sub-frames in these  
72 tests are non-seismically designed, indicating the relatively weak collapse-resistant capacity of non-  
73 seismically designed RC frames, which calls for efficient strengthening schemes to improve their  
74 robustness.

75 Using externally bonded carbon/glass fiber reinforced polymer (CFRP/GFRP) strips or sheets is an  
76 effective way to enhance the performance of RC components [18-21]. Karayannis and Goliass [18] and  
77 Goliass et al. [19] used CFRP ropes as external reinforcements to strengthen the RC beam-column joints  
78 and found that the strengthened joints exhibited improved structural performance. Chalioris et al. [20]  
79 and Kakaletsis et al. [21] summarized the techniques for strengthening RC components, such as the  
80 utilization of CFRP U-shaped jackets and plates. In recent years, CFRP/GFRP materials have been  
81 employed to strengthen the collapse-resistant capacity of RC structures [22-27]. Kim et al. [23] applied  
82 CFRP strips to the side or soffit of the beams for providing continuity to the beams, it was found that both  
83 CFRP anchors and CFRP U-wraps can efficiently anchor the CFRP strips. Qian and Li [24] and Feng et  
84 al. [26] investigated the merits of externally bonded GFRP strips to enhance the performance of RC beam-  
85 slab sub-structures subjected to an interior and a corner column missing scenario, respectively. Liu et al.

86 [25] adopted CFRP cables to retrofit the collapse-resistant capacity of a 1/2 scale RC structure. It was  
87 found that the RC structure could obtain a new balance after the sudden loss of two edge columns.  
88 Elsanadedy et al. [27] used CFRP U-wraps to strengthen the dry connections of the precast concrete sub-  
89 frame, it was found that the upgraded sub-frame had a similar ultimate load capacity to the RC sub-frame.

90 To enhance the collapse-resistant capacity of non-seismically designed RC frames using CFRP  
91 strengthening technique, an experimental program including two referential RC sub-frames and five  
92 strengthened RC sub-frames with CFRP is conducted in this paper. The strengthening schemes aim to  
93 increase either CAA capacity or CA capacity, or both the CAA and CA capacities. In addition, available  
94 test results in terms of the plastic rotations of the beam ends are collected to compare with the acceptable  
95 performance criteria in existing codes for collapse-resistant design. Based on the test results and  
96 comparative study, design recommendations for collapse-resistant design of RC buildings were made.

## 97 **2. Experimental Program**

### 98 *2.1 Sub-frame design and material property*

99 The design of the prototype RC building follows the building code ACI 318-19 [28]. The design  
100 dead load and live load are 5.5 kPa and 2.0 kPa, respectively. Seven sub-frames were extracted from the  
101 prototype building and scaled down to 1/2 as specimens for test. The information on the experimental  
102 program is listed in **Table 1**. The sub-frames are categorized into two groups based on the removed  
103 columns. Group 1 consists of three sub-frames under the loss of a penultimate column (P-R, P-S-C, and  
104 P-S-CC) whereas Group 2 includes four sub-frames subjected to the loss of an edge column (E-R, E-S-  
105 C, E-S-CC1, and E-S-CC2). In the notations of sub-frames, the first letter P or E denotes the removed  
106 columns; the second letter R or S indicates referential or strengthened sub-frames; the third letter C and  
107 the fourth letter C (if any) mean CAA and CA, respectively. The geometric dimension and reinforcement  
108 arrangement of the sub-frames are shown in **Fig. 1**. The beam was 2750 mm in length. The sectional  
109 dimensions of the beam and the column were 150 mm×250 mm and 250 mm×250 mm, respectively.  
110 Ribbed reinforcing bars with diameters of 10 mm (T10) and 12 mm (T12) were used as the longitudinal  
111 rebar of the beams and columns, respectively. Round bars with a diameter of 6 mm and a spacing of 100  
112 mm were arranged along the beams. The beams were extended from both side joints for the sub-frames  
113 subjected to the edge column removal scenario. The extended beams were designed to simulate the axial

114 constraints from adjacent bays. In contrast, sub-frames under the penultimate column removal scenario  
115 were in asymmetric boundary conditions, only the beam on the left side was extended from the side joint.  
116 Compared with seismically designed frames, the frames studied here had relatively lower reinforcement  
117 ratio. Moreover, the sum of flexural strengths of columns shall be greater than 1.2 times the sum of  
118 flexural strengths of the beams for seismically designed frames (ACI 318-19 [28]). However, in this study,  
119 the ratio of the sum of flexural strengths of columns to the sum of flexural strengths of the beams was  
120 1.1.

121 **Table 2** lists the material properties of the reinforcement and CFRP. The concrete used to cast the  
122 sub-frames has an average cylinder compressive strength of 36.4 MPa and an average splitting tensile  
123 strength of 3.3 MPa. In addition, the maximum aggregate size of the concrete is 10 mm.

## 124 ***2.2 Test setup and instrumentation***

125 **Fig. 2** shows the test setup. The test setup and installation of the two groups of sub-frames are similar.  
126 The top of the side column and the extended beam were linked to the reaction frame via horizontal  
127 constraints, the side column base was pinned to the strong ground of the laboratory. The targeted column  
128 was notionally removed before testing. Hydraulic jack 1 (Item 3) and a steel assembly (Item 5) were  
129 installed to ensure in-plane loading of the sub-frames. To account for the effect of gravity load from the  
130 upper stores, hydraulic jack 2 (Item 7) was installed to implement an axial compression ratio of 0.2 to the  
131 side columns. At the beginning of the test, constant axial compression was first applied to the side  
132 columns, and then a displacement-control loading scheme was used to apply load to the top of the target  
133 column by the hydraulic jack with a loading rate of 0.5 mm/min.

134 Two load cells (Items 2 and 4) were installed along the axis of hydraulic jack 1 to measure the load  
135 applied to the sub-frames. Tension/compression load cells and load pins were installed in the horizontal  
136 constraints and pin supports to monitor the horizontal reaction forces. In addition, a series of seven linear  
137 variable displacement transducers (LVDTs, Item 6) were arranged along the length of the beams to record  
138 the deflection of the beams; another series of ten LVDTs (Item 9) were installed along the height of the  
139 two side columns to record their horizontal movement. Moreover, strain gauges were mounted to the  
140 reinforcement and CFRP strips.

### 141 3. Test Results of Referential Sub-frames

#### 142 3.1 Load resistance and failure mode

143 **Fig. 3a** shows the load resistance-displacement history of the referential sub-frames while **Table 3**  
144 lists the critical test results. The overall trend of the load resistance-displacement history was consistent  
145 with the results from available tests of non-seismically designed RC sub-frames [3, 10, 13]. The load  
146 resistance was dominated by the CAA capacity. A severe load resistance softening occurred after the  
147 CAA capacity, after which was a limited development of CA. The YL/CAA capacities of P-R and E-R  
148 were 33 kN/42 kN and 35 kN/45 kN, respectively. Therefore, the enhancement ratios of CAA were 1.27  
149 and 1.29, respectively. The first rebar fracture occurred in the beam bottom rebar near the removed  
150 column at the displacements of 125 mm and 150 mm for P-R and E-R, respectively. Then, consecutive  
151 fracture of the tension rebar of beam ends was measured. Accordingly, the load resistance of the two sub-  
152 frames decreased continuously as the beam ends lost the bending moment capacity. The load resistance  
153 gained a limited increase because of CA. However, the CA capacities of P-R and E-R were 33 kN and 40  
154 kN, respectively, less than the CAA capacities.

155 **Fig. 4** and **Fig. 5** show the failure modes of P-R and E-R, respectively. The beam tension rebars at  
156 the beam ends were fractured except that of the beam end near the left-side column. The distributed cracks  
157 along the beams indicated that the beams were in tension at the end of the tests. Moreover, hairline flexural  
158 cracks were formed in the exterior side of the side columns because the axial compression of the beam at  
159 the CAA stage pushed the side column to move outward. Different from ER, extensive cracks were  
160 formed in the right-side column of PR at the CA stage due to the absence of the extended beam.

#### 161 3.2 Horizontal reaction force

162 **Fig. 6a** illustrates the horizontal reaction force-displacement relationship of P-R and E-R. Horizontal  
163 compressive reaction forces (HCRF) were first measured. The maximum HCRFs on the left side and right  
164 side of PR were -76 kN and -61 kN, respectively. Therefore, the presence of the extended beam could  
165 increase the maximum HCRF by 24.6%. The maximum HCRF of ER was -82 kN, which was 7.9% greater  
166 than that of PR. When the rebar fractured at the CAA stage, the HCRF only experienced a mild variation.  
167 When the CA kicked in, the HCRF converted to horizontal tensile reaction force (HTRF). The maximum  
168 HTRFs on the left side and right side of P-R were 90 kN and 73 kN, respectively. The maximum HCRF  
169 of E-R was 102 kN, which was 13.3% greater than that of P-R.

### 170 **3.3 Deflection of the beam and side column**

171 **Fig. 7** demonstrates the deflection of the beam of E-R. It can be seen that the beams exhibited visible  
172 flexural deformation at the beam ends whereas the middle segment of the beams almost kept straight. At  
173 the final of the test, the deflection shape of the left side beam was similar to a cantilever beam because  
174 the beam end near the left side column was still able to sustain bending moment. Differently, since the  
175 beam tension rebar of the beam ends fractured completely, the whole right-side beam kept straight.  
176 Similar observation was obtained in P-R. **Fig. 8** compares the deflection of the right-side column (without  
177 extended beam) of E-R and P-R. The side column moved outward at the CAA stage because of the axial  
178 compression in the beams. Afterward, the side columns began to move inward to respond to the axial  
179 tension of the beams at the CA stage. The maximum outward movements of the right-side column of E-  
180 R and P-R were -5.1 mm and -6.5 mm, respectively, whereas the maximum inward movements were 5.4  
181 mm and 7.6 mm, respectively.

## 182 **4. Strengthening Schemes**

183 Based on the test results of the referential sub-frames, the main weaknesses of non-seismically  
184 designed RC frames under a column removal scenario are summarized as follows: (1) relatively low beam  
185 reinforcement ratio leads to the premature fracture of the beam rebar at the CAA stage, which in turn  
186 results in a severe load softening; (2) due to the same reason, the CA gains limited development; (3) the  
187 exterior beam-column joint (without constraint from the extended beam) can suffer severe damage.  
188 Therefore, five strengthening schemes with CFRP were developed in this paper to improve their collapse-  
189 resistant capacity, as shown in **Fig. 9**. The number in **Fig. 9** indicates the construction steps. The  
190 strengthening schemes were designed in accordance with ACI 440.2R-17 [29], the details of each  
191 strengthening scheme was presented below.

### 192 **4.1 P-S-C**

193 **Fig. 9a** demonstrates the strengthening scheme of P-S-C. This sub-frame was strengthened to  
194 achieve a higher CAA capacity. First, L-shaped CFRP strips with a branch length of 500 mm were applied  
195 to the beam ends and columns. It should be noted that the 500 mm length was designed considering the  
196 length of potential plastic hinge was 250 mm (one beam depth) and the additional length of 250 mm for  
197 anchorage. The anchorage length of 250 mm was greater than the requirement of ACI 440.2R-17 [29]. A

198 straight CFRP strip with 1250 mm in length and 150 mm in width was applied on the exterior face of the  
199 right side column to enhance the bending moment capacity of the beam ends and columns (Item ①);  
200 Second, CFRP wraps were applied to the columns with a spacing of 150 mm for enhancing the columns  
201 and providing anchorage to the L-shaped strips (Item ②); Third, CFRP strips with 200 mm in height were  
202 applied to the side of beam-column joints to improve the shear strength of joints (Item ③, not reaching  
203 the height of the beam considering the presence of slabs in practical buildings); Fourth, U-shaped CFRP  
204 wraps with 150 mm in width were applied to the beam ends to enhance the anchorage of the horizontal  
205 branch of the L-shaped CFRP strips as suggested by Kim et al. [23] (Item ④). Both the CFRP strips and  
206 wraps were two layers, and epoxy was used for bonding CFRP.

#### 207 **4.2 P-S-CC**

208 As shown in **Fig. 9b**, on the basis of the strengthening scheme of P-S-C, additional two layers of  
209 continuous CFRP strips were first applied to the soffit of the beams of P-S-CC for providing continuity,  
210 which was expected to be able to enhance the CA capacity. To ensure continuity, the CFRP strips were  
211 divided by two at the beam-column interfaces and threaded through two pre-drilled holes in the columns,  
212 as suggested by previous studies [22, 23].

#### 213 **4.3 E-S-C**

214 E-S-C was strengthened to obtain a higher CA capacity. As shown in **Fig. 9c**, the continuous CFRP  
215 strips were applied to the soffit of the beams, and U-shaped CFRP wraps were applied to the beam ends  
216 to prevent the delamination of the continuous CFRP strip.

#### 217 **4.4 E-S-CC1 and E-S-CC2**

218 The strengthening schemes of E-S-CC1 and E-S-CC1 are shown in **Fig. 9d**. The strengthening  
219 details of E-S-CC1 were similar to that of P-S-CC. However, for E-S-CC2, the L-shaped CFRP strips, U-  
220 shaped CFRP wraps, and CFRP strips on the side of the beam-column joints were changed to one layer.  
221 Moreover, the CFRP wraps on the columns were changed to three layers.

### 222 **5. Test Results of Strengthened Sub-frames**

#### 223 **5.1 Load resistance and failure mode**

##### 224 **P-S-C and P-S-CC**

225 The load resistance-displacement histories of P-S-C and P-S-CC are shown in **Fig. 3b** and the critical  
226 test results are listed in **Table 3**. It can be seen that the overall trend of the load resistance-displacement  
227 histories of P-S-C and P-S-CC was similar to that of P-R. Compared with P-R, the YL capacities of P-S-  
228 C and P-S-CC were increased by 21.2% and 33.3%, namely, 40 kN and 44 kN, respectively. Moreover,  
229 the CAA capacities of P-S-C and P-S-CC were increased by 16.7% and 23.8%, i.e., 49 kN and 52 kN,  
230 respectively. However, severe load softening also occurred in P-S-C and P-S-CC, in particular for P-S-C.  
231 Different from P-R, for P-S-C, the first rebar fracture occurred in the beam top rebar near the right-side  
232 column at a displacement of 183 mm. Subsequently, consecutive fracture of the tension rebar of the beam  
233 ends was observed. As a result, the L-shaped CFRP strips began to de-bond and the CFRP wraps on the  
234 column ruptured. At a displacement of 290 mm, the beam bottom rebar near the removed column  
235 fractured completely, resulting in debonding of L-shaped strips, which in turn led to the rupture of the  
236 overlying CFRP wraps on the removed column. Consequently, the beam ends of P-S-C could not sustain  
237 bending moment anymore, and the load resistance within the displacement from 280 mm to 310 mm was  
238 closed to zero. The load resistance of P-S-C could reascend but drop to zero after reaching the CA capacity  
239 of 24 kN, which was 27.3% less than that of P-R. For P-S-CC, the CAA capacity was followed by an  
240 immediate drop in load resistance, which was ascribed to the slight debonding of the continuous CFRP  
241 strip near the removed column. The beam bottom rebar near the removed column fractured first at a  
242 displacement of 172 mm. However, the continuous CFRP strip prevented the complete fracture of beam  
243 bottom rebar near the removed column, therefore, P-S-CC did not lose its load resistance even though the  
244 beam top rebar near the side columns fractured completely. At the final, partial continuous CFRP strip  
245 near the removed column was ruptured. The CA capacity of P-S-CC of 55 kN was achieved at a  
246 displacement of 621 mm, which was 66.7% greater than that of P-R.

247 **Fig. 10** and **Fig. 11** show the failure modes of P-S-C and P-S-CC, respectively. Extensive cracks  
248 penetrated the beams depth, rebar fracture occurred at the beam ends, side CFRP strips were ruptured, L-  
249 shaped CFRP strips suffered debonding and caused the rupture of the overlying CFRP wraps on the  
250 columns. The beam rebar of the beam end near the right-side column fractured completely for P-S-C, but  
251 not for P-S-CC due to the present continuous CFRP strip. In addition, the distribution of the cracks along  
252 the beams of P-S-CC was sparser than P-S-C. Compared with the failure mode of P-R (**Fig. 4**), the side

253 columns of P-S-C and P-S-CC suffered much milder damage, in particular for the right side column, only  
254 one crack was observed.

### 255 **E-S-C, E-S-CC1, and E-S-CC2**

256 The load resistance-displacement histories of E-S-C, E-S-CC1, and E-S-CC2 are shown in **Fig. 3c**.  
257 The YL capacities of E-S-C, E-S-CC1, and E-S-CC2 were 36 kN, 47 kN and 42 kN, respectively,  
258 corresponding to the increasements of 2.9%, 34.3%, and 20.0% compared with E-R, respectively. The  
259 CAA capacities of E-S-C, E-S-CC1, and E-S-CC2 were 47 kN, 58 kN and 53 kN, respectively,  
260 corresponding to the increasements of 4.4%, 28.9%, and 17.8% compared with E-R, respectively. For E-  
261 S-C, the beam bottom rebar near the removed column was first to fracture at a displacement of 193 mm.  
262 The test of E-S-C was stopped due to consecutive fracture of beam top rebar near the side column. The  
263 CA capacity of 46 kN was measured at a displacement of 567 mm, which was 15.0% greater than that of  
264 E-R. E-S-CC1 and E-S-CC2 obtained their CA capacities of 58 kN and 49 kN at the displacement of 597  
265 mm and 577 mm, respectively, which were 145.0% and 122.5% of that of E-R, respectively.

266 **Fig. 12, Fig. 13, and Fig. 14** give the failure modes of E-S-C, E-S-CC1, and E-S-CC2, respectively.  
267 In general, the failure mode of E-S-C was similar to that of E-R except that more cracks formed in the  
268 side column because of the additional tensile force from the continuous CRFP strip. The failure mode of  
269 E-S-CC1 was analogous to that of P-S-CC: extensive cracks developed along the beams, rebar fracture  
270 occurred at the beam ends, L-shaped CFRP strips suffered debonding and the overlying CFRP wraps on  
271 the columns were ruptured. However, no debonding occurred in the L-shaped CFRP strip of E-S-CC2,  
272 and the CFRP wraps were intact at the end of test. This is because both the L-shaped CFRP strips and  
273 CFRP wraps on columns of E-S-CC1 were two layers, whereas the L-shaped CFRP strips and CFRP  
274 wraps on columns of E-S-CC2 were one layer and three layers, respectively.

### 275 **5.2 Horizontal reaction force**

276 The horizontal reaction force-displacement curves of the strengthened sub-frames are shown in **Fig.**  
277 **6**. The left/right side maximum HCRFs of P-S-C and P-S-CC were -91/-78 kN and -98/-85 kN,  
278 respectively, indicating the increasements of 19.7/27.9% and 28.9/39.3% compared with P-R,  
279 respectively. The maximum HTRFs of P-S-C and P-S-CC were 67/58 kN and 125/113 kN, respectively.  
280 Therefore, P-S-C obtained the lowest maximum HTRF, which agreed well with the load resistance. The  
281 maximum HCRFs of E-S-C, E-S-CC1, and E-S-CC2 were -87 kN, -111 kN, and -101 kN, respectively.

282 Compared with E-R, the maximum HCRFs of E-S-C, E-S-CC1, and E-S-CC2 were higher by 6.1%,  
283 35.4%, and 23.2%, respectively. The maximum HTRFs of E-S-C, E-S-CC1, and E-S-CC2 were 111 kN,  
284 138 kN, and 119 kN, respectively, which were 8.8%, 35.3%, and 16.7% higher than that of E-R,  
285 respectively.

### 286 **5.3 Strain of CFRP strips**

287 **Fig. 15** presents the strains of the CFRP strips of P-S-C and P-S-CC at the stage of CAA. The strain  
288 of the CFRP strip bonded on the exterior face of the right-side column was in tension as a result of the  
289 outward deflection of the side column due to beam compressive axial force. Besides, the CFRP strips  
290 were proved to have been properly bonded on the tensile zone of the beam ends since considerable tensile  
291 strain developed there, confirming the effectiveness of the proposed strengthening schemes for improving  
292 the flexural capacity of beams. Similar results were obtained for other specimens.

## 293 **6. Discussion**

### 294 **6.1 Efficiency of the strengthening schemes**

295 As tabulated in **Table 3**, the YL/CAA/CA capacities of P-R, P-S-C, and P-S-CC were 33/42/33 kN,  
296 40/49/24 kN, and 44/52/55 kN, respectively. Compared with the referential sub-frame P-R, the  
297 YL/CAA/CA capacities of P-S-C and P-S-CC were increased by 21.2%/16.7%/-27.3% and 33.3%  
298 /23.8%/66.7%, respectively. Therefore, the strengthening schemes effectively enhance the collapse-  
299 resistant capacity of P-S-C and P-S-CC at the YL and CAA stages. However, P-S-C achieved the lowest  
300 CA capacity among these three sub-frames, this will be discussed below. The YL/CAA/CA capacities of  
301 E-R, E-S-C, E-S-CC1, and E-S-CC2 were 35/45/40 kN, 36/47/46 kN, 47/58/58 kN, and 42/53/49 kN,  
302 respectively, which were 2.9%/4.4%/15.0%, 34.3% /28.9%/45.0%, and 20.0% /17.8%/22.5% higher than  
303 that of the referential sub-frame E-R, respectively. The deformation capacity, which was defined as the  
304 displacement at CA capacity, of P-R, P-S-C, and P-S-CC was 552 mm, 560 mm, and 621 mm,  
305 respectively. The strengthening scheme aiming at increasing CAA capacity had a marginal effect on the  
306 deformation capacity of the sub-frame subjected to a penultimate column removal scenario whereas the  
307 strengthening scheme designed to enhance both CAA and CA capacity increased the deformation  
308 capacity by 12.5%. The deformation capacity of E-R, E-S-C, E-S-CC1, and E-S-CC2 was 532 mm, 567  
309 mm, 597 mm, and 577 mm, respectively. The strengthening scheme aiming at increasing CA capacity

310 increased the deformation capacity of the sub-frame subjected to an edge column removal scenario by  
311 6.6% whereas the strengthening scheme designed to improve both CAA and CA capacity increased the  
312 deformation capacity by 8.5% to 12.2%.

313 In summary, the strengthening schemes could effectively improve the collapse-resistant capacity of  
314 the sub-frames. However, as shown in **Fig. 3**, the load resistance of the strengthened sub-frames at the  
315 transition stage is even lower than that of the referential sub-frames, indicating that the strengthening  
316 schemes failed to alleviate the severe load resistance softening. This is because the application of CFRP  
317 resulted in the strain concentration at the beam ends, and the detrimental influence of the strain  
318 localization aggravated the premature fracture of beam rebar. In this case, P-S-C obtained the lowest CA  
319 load resistance and deformation capacity. However, sub-frames with continuous CFRP strip were capable  
320 of further developing CA.

321 Compared with P-R, the fewer cracks in the right-side columns of P-S-C and P-S-CC demonstrated  
322 that the CFRP wraps could mitigate the damage to the columns. The L-shaped CFRP strips experienced  
323 debonding and resulted in the rupture of the overlying CFRP wraps on the columns for the strengthened  
324 sub-frames except for E-S-CC2. In contrast, for E-S-CC2, the L-shaped CFRP strips were fractured  
325 whereas the CFRP wraps were intact. In this study, the CFRP wraps were used to provide anchorage to  
326 the L-shaped CFRP strips, and therefore, the failure mode of E-S-CC2 was more preferent. In E-S-CC2,  
327 the layer number of the CFRP wraps was three times that of the L-shaped CFRP strips. However, the  
328 layer number of the CFRP wraps and the layer number of the L-shaped CFRP strips in the other  
329 strengthened sub-frames were equal.

## 330 **6.2 Dynamic collapse-resistant capacity**

331 The static load resistance recorded in the test shall be transformed into the dynamic load resistance  
332 due to the dynamic nature of progressive collapse. In this section, the transformation was implemented  
333 with the energy-based framework proposed by Izzuddin et al. [30]. As illustrated in **Fig. 16**, the strain  
334 energy  $W_s$  in the remaining structure in the event of zero kinetic energy is equal to the work  $W_g$  done by  
335 the concentrated load. Thus, the pseudo-static load resistance, i.e., dynamic load resistance, can be  
336 obtained by dividing the area under the measured quasi-static load-displacement curve by the  
337 displacement. **Fig. 17** shows the dynamic collapse-resistant capacities of the sub-frames. The peak  
338 dynamic collapse-resistant capacities of P-R, P-S-C, P-S-CC, E-R, E-S-C, E-S-CC, and E-S-CC2 were

339 35 kN, 44 kN, 43 kN, 39 kN, 41 kN, 51 kN, and 46 kN, respectively. It can be seen that the overall trend  
340 of dynamic load resistance-displacement histories of the sub-frames was different from that of static ones.  
341 The peak dynamic load resistances were attained at the CAA stage, and no obvious reascending behavior  
342 was observed after the load resistance softening. Therefore, whilst the CA capacities of P-S-CC and E-  
343 E-S-CC2 were higher than the CAA capacities, their peak dynamic collapse-resistant capacities were  
344 achieved at the CAA stage. This is because the severe load resistance softening could result in an  
345 appreciable amount of kinetic energy of the beams during collapse while the development of CA was too  
346 limited to consume all the kinetic energy. Therefore, it was concluded that the strengthened CA capacity  
347 failed to increase the dynamic collapse-resistant capacity, however, it can change the collapse mode of  
348 buildings due to increased energy dissipation capacity. Moreover, DoD [31] suggests that the use of  
349 composite materials such as FRP to provide the tie forces is acceptable when the FRP can meet the  
350 rotation requirement of 0.20 rad. However, although the rotational capacity of the beams of P-S-CC, E-  
351 S-CC1, and E-S-CC2 exceeded 0.2 rad, test results indicated that no reliable tie force was achieved .

### 352 ***6.3 Acceptable performance criteria for collapse-resistant design***

353 DoD [31] and GSA [32] provide acceptable performance criteria (plastic rotation of beam end  $[\theta]$ )  
354 for RC beams governed by flexural behavior at the collapse prevention level. The acceptance criteria  
355 depend on the indicators  $(\rho - \rho') / \rho_{\text{bal}}$ ,  $V / b_w d \sqrt{f'_c}$ , and the ratio of stirrup spacing to effective beam  
356 depth, where  $\rho$ ,  $\rho'$  and  $\rho_{\text{bal}}$  are tension, compression, and balanced reinforcement ratios of beam  
357 critical section, respectively;  $V$  is design shear force;  $b_w$  and  $d$  are web width and effective depth of  
358 beam;  $f'_c$  is compressive strength of concrete. The beams are categorized into conforming and  
359 nonconforming (C and NC) beams depending on the hoop spacing within the plastic hinge region. If the  
360 hoops are spaced at  $\leq d/3$ , the beams are conforming, otherwise, nonconforming. The C and NC beams  
361 can be approximately considered seismically and non-seismically designed beams, respectively, because  
362 the maximum hoop spacing of seismically designed beams is explicitly required to be less than or equal  
363 to  $d/4$  [28, 33]. The acceptance criteria for primary and secondary components are different for DoD [31],  
364 but not for GSA [32]. In DoD [31], stricter acceptance criteria are stipulated for the primary component.  
365 In GSA [32], the acceptance criteria of the primary and secondary components are the same and are equal

366 to the acceptance criteria of the secondary component in DoD [31]. More details can be found in Table 6  
367 in GSA [32] and Table 4-1 in DoD [31].

368 To assess the acceptable performance criteria for collapse prevention, a database including 113 test  
369 results was built based on available papers to conduct a comparative study [2-5, 7, 9-13, 34-49]. The  
370 information on the collected tests is listed in **Table 4**. Since the information on the design loads was not  
371 provided in many papers, the indicator  $V / b_w d \sqrt{f'_c}$  was taken less than or equal to 0.25, units in MPa.  
372 As shown in **Table 4**, the measured plastic rotation of the beam end at the CAA capacity  $\theta_{CAA}$ , which was  
373 determined by subtracting the chord rotation of the beam at the YL capacity  $\theta_y$  from the  $\theta_{CAA}$ , was  
374 compared with the acceptance criteria. The chord rotation of the beam is defined as the ratio of removed  
375 column displacement to beam's clear span. For the tests without information about YL, the measured  $\theta_{CAA}$   
376 was approximately determined by the chord rotation of the beam at the CAA capacity. As listed in **Table**  
377 **4** and **Fig. 18**, the measured  $\theta_{CAA}$  fall in the acceptable range of both GSA [32] and DoD [31]. In other  
378 words, the CAA is supposed to be a reliable defense line against collapse.

379 The above acceptable performance criteria at the collapse prevention level are for RC beams  
380 controlled by flexure, which means the collapse of building is preferred to be prevented at flexural stage.  
381 However, this may be too conservative if considerable CA can be developed in the beams. The beams  
382 undergoing CA, which transfer the loads from the damaged region of the building to the undamaged  
383 portion via tie forces rather than flexure, are controlled by axial tensile force. To date, related acceptable  
384 performance criteria are not clear. DoD [31] stipulates that unless the beams and their connections can be  
385 shown capable of carrying the required tie force while undergoing rotations of 0.2 rad, the tie forces are  
386 to be carried by the floor and roof system. Among the 113 tests, only 55 tests (48.7%) demonstrated a  
387 superior CA capacity to CAA capacity. As shown in **Fig. 19**, in general, the beams in these 55 tests were  
388 able to provide 0.2 rads. In other words, 0.2 rad rotational capacity of the beams can ensure considerable  
389 CA capacity. Unfortunately, no explicit method is available to judge whether the beams can provide 0.2  
390 rads due to various influential parameters.

391 In reality, the conclusions on the reliability of CA to work as the second defense line to resist  
392 collapse are inconsistent owing to different specimens. Yu and Tan [7] and Yu and Tan [13] conducted  
393 tests of RC beam-column assemblies with similar geometric dimensions and reinforcing details but

394 different side columns, the former used simplified enlarged side columns, whereas the latter adopted  
395 scaled side columns, similar to the current study. It was found that, due to the absence of axial  
396 compression in the side columns, the simplified enlarged side columns can result in overestimated  
397 rotational capacity of the beam ends near the side columns and CA capacity. In comparison, the rotational  
398 capacity of the beam ends of assemblies with scaled side columns was less. This is because the axial  
399 compression ratios of 0.4 to 0.6 of the scaled side columns put the longitudinal rebar of the beams in a  
400 higher bond stress regime, which resulted in premature rebar fracture and lower CA capacity. However,  
401 in Qian et al. [47] and Qian et al. [49]'s tests, comparable rotational capacities of the beam ends and CA  
402 capacities were measured for the assemblies with simplified enlarged side columns and scaled side  
403 columns, which may be attributed to the relatively lower axial compression ratio of 0.3 of the scaled side  
404 columns. Moreover, the development of CA depends on boundary conditions, reinforcement ratio, and  
405 span-to-depth ratio of the beams, which are various in buildings. In summary, it is reasonable to exclude  
406 CA from the acceptable load-resisting mechanism to mitigate collapse until explicit method for  
407 determination of the rotational capacity of beams is proposed.

#### 408 **6.4 A simple collapse-resistant design method**

409 To improve the current collapse-resistant design, a simple design method was proposed, which  
410 included two steps: First, determining the load resistance function of critical components of the target  
411 frame, i.e., sub-frame; Second, determining the dynamic collapse-resistant capacity based on the load  
412 resistance function. As shown in **Fig. 20**, the load resistance function was assumed to be trilinear and  
413 featured three key points: points  $(d_y, P_y)$ ,  $(d_{CAA}, P_{CAA})$ , and  $(d_u, P_u)$ .  $P_y$ ,  $P_{CAA}$ , and  $P_u$  indicate YL, CAA  
414 capacity, and ultimate load at the acceptable performance criterion, respectively, and  $d_y$ ,  $d_{CAA}$ , and  $d_u$   
415 indicate the displacement at YL, CAA capacity, and ultimate load, respectively. The load resistance after  
416 the acceptable performance criterion was neglected to obtain a conservative design.  $P_y$  is calculated by  
417 **Eq. 1**. The nominal flexural strength of the beam section  $M_y$  can be calculated by **Eq. 2** [50].

$$418 \quad P_y = \frac{2(M_{y1} + M_{y2})}{l_n} \quad (1)$$

$$419 \quad M_y = \rho f_y d^2 (1 - 0.59 \rho f_y / f_c) \quad (2)$$

$$420 \quad d_y = \frac{M_y}{0.3 E_c I} l_n \quad (3)$$

421 where  $M_{y1}$  and  $M_{y2}$  are the nominal flexural strengths of the two beam ends of a beam;  $l_n$  is the clear span  
 422 of the beam;  $\rho$  is the tension reinforcement ratio;  $f_y$  is the yield strength of tension reinforcement;  $d$  is the  
 423 effective beam depth;  $f_c$  is the cylinder compressive strength of concrete;  $0.3E_cI$  is the effective flexural  
 424 rigidity of RC beam as suggested by ASCE-41 [51];  $I$  is the inertial moment of beam section; and  $E_c$  is  
 425 the elastic modulus of concrete.

426 An important challenge is to calculate  $P_{CAA}$ . For the beams with insufficient axial constraint (YL  
 427 dominated), like the beams under a corner column removal scenario,  $P_{CAA}$  can be taken as  $P_y$ . For the  
 428 beams with sufficient axial constraint (CAA dominated),  $P_{CAA}$  can be calculated by existing CAA model  
 429 [52, 53], and  $d_{CAA}$  is suggested to be  $0.033l_n$  based on the average value of the measured values of the  
 430 database. Based on the discussion in Section 6.3, the acceptance criterion was suggested to be 0.063 rad  
 431 because such a criterion included almost all CAA capacities of the database. Therefore,  $d_u$  is calculated  
 432 as  $(d_y+0.063l_n)$ .  $P_u$  can be assumed to be equal to  $P_y$ . Based on the determined load resistance function  
 433 and energy method [30], the dynamic collapse-resistant capacity  $P_d$  is obtained as **Eq. 4**. Besides the  
 434 energy method, single degree of freedom model can be used to conduct nonlinear dynamic analysis to  
 435 obtain  $P_d$  [16, 54].

$$436 \quad P_d = \frac{0.5P_y d_y + 0.5(P_y + P_{CAA})(d_{CAA} - d_y) + 0.5(P_{CAA} + P_u)(d_u - d_{CAA})}{d_u} \quad (4)$$

## 437 7. Conclusions

438 An experimental program was carried out to enhance the collapse-resistant capacity of non-  
 439 seismically designed RC frames using various CFRP strengthening schemes. Moreover, existing  
 440 acceptance criteria for collapse prevention were compared with numerous test results. Based on the test  
 441 results and discussion, the main conclusions were drawn as follows:

- 442 1. The strengthening schemes can effectively enhance the collapse-resistant capacity of P-S-C and  
 443 P-S-CC at the CAA and CA stages. The YL/CAA/CA capacities of P-S-C and P-S-CC were  
 444 21.2%/16.7%/-27.3% and 33.3% /23.8%/66.7% higher than that of the referential sub-frame P-  
 445 R, respectively. The YL/CAA/CA capacities of E-S-C, E-S-CC1, and E-S-CC2 were  
 446 2.9%/4.4%/15.0%, 34.3% /28.9%/45.0%, and 20.0% /17.8%/22.5% higher than that of the  
 447 referential sub-frame E-R, respectively.

- 448 2. On the one hand, the strengthening schemes could increase the collapse-resistant capacity of the  
449 sub-frames. On the other hand, the strengthening schemes could aggravate premature rebar  
450 fracture due to strain localization of the beams, leading to a higher CAA capacity but lower CA  
451 capacity and deformation capacity, such as P-S-C.
- 452 3. Whilst the CA capacities of P-S-CC, E-S-C, E-S-CC1, and E-S-CC2 were equal to or higher  
453 than their CAA capacities, the dynamic collapse-resistance capacities of these sub-frames were  
454 obtained at the CAA stage, indicating that the strengthened CA capacity was unable to increase  
455 the dynamic collapse-resistance, which can be attributed to the severe softening of load  
456 resistance.
- 457 4. The comparison of the acceptance criteria and measured plastic rotations of the beam ends at  
458 the CAA capacity demonstrated that CAA is an acceptable mechanism for collapse prevention.  
459 If the beams can ensure 0.2 rad rotational capacity, considerable CA capacity can be obtained.  
460 However, the lack of methods to determine the rotational capacity of the beams makes CA  
461 unreliable in collapse-resistant design.

## 462 **Acknowledgments**

463 The authors gratefully acknowledge the financial support provided by the National Natural Science  
464 Foundation of China (Nos. 51778153 and 52022024). Any opinions, findings and conclusions expressed  
465 in this paper do not necessarily reflect the view of the National Natural Science Foundation of China.

## 466 **References**

- 467 [1] ASCE-7 ASCE 7-16 Minimum Design Loads and Associated Criteria for Buildings and Other  
468 Structures. 2016.
- 469 [2] Su YP, Tian Y, Song XS. Progressive collapse resistance of axially-restrained frame beams. *ACI*  
470 *Structural Journal* 2009;106(5):600-8.
- 471 [3] Choi H, Kim J. Progressive collapse-resisting capacity of RC beam–column sub-assembly.  
472 *Magazine of Concrete Research* 2011;63(4):297-310.
- 473 [4] Sadek F, Main JA, Lew HS, Bao YH. Testing and analysis of steel and concrete beam-column  
474 assemblies under a column removal scenario. *Journal of Structural Engineering* 2011;137(9):881-  
475 92.

- 476 [5] Farhang Vesali N, Valipour H, Samali B, Foster S. Development of arching action in longitudinally-  
477 restrained reinforced concrete beams. *Construction and Building Materials* 2013;47:7-19.
- 478 [6] Stinger SM, Orton SL. Experimental evaluation of disproportionate collapse resistance in reinforced  
479 concrete frames. *ACI Structural Journal* 2013;110(3):521-9.
- 480 [7] Yu J, Tan KH. Structural behavior of RC beam-column subassemblages under a middle column  
481 removal scenario. *Journal of Structural Engineering* 2013;139(2):233-50.
- 482 [8] Qian K, Li B. Dynamic performance of RC beam-column substructures under the scenario of the loss  
483 of a corner column—Experimental results. *Engineering Structures* 2012;42:154-67.
- 484 [9] Qian K, Li B. Performance of three-dimensional reinforced concrete beam-column substructures  
485 under loss of a corner column scenario. *Journal of Structural Engineering* 2013;139(4):584-94.
- 486 [10] Vali pour H, Vessali N, Foster SJ, Samali B. Influence of concrete compressive strength on the  
487 arching behaviour of reinforced concrete beam assemblages. *Advances in Structural Engineering*  
488 2015;18(8):1199-214.
- 489 [11] Deng XF, Liang SL, Fu F, Qian K. Effects of high-strength concrete on progressive collapse  
490 resistance of reinforced concrete frame. *Journal of Structural Engineering* 2020;146(6):04020078.
- 491 [12] Kang SB, Tan KH. Robustness assessment of exterior precast concrete frames under column removal  
492 scenarios. *Journal of Structural Engineering* 2016;142(12):04016131.
- 493 [13] Yu J, Tan KH. Structural behavior of reinforced concrete frames subjected to progressive collapse.  
494 *ACI Structural Journal* 2017;114(1):63-74.
- 495 [14] Qian K, Li B. Effects of masonry infill wall on the performance of RC frames to resist progressive  
496 collapse. *Journal of Structural Engineering* 2017;143(9):04017118.
- 497 [15] Qian K, Liang SL, Fu F, Fang Q. Progressive collapse resistance of precast concrete beam-column  
498 sub-assemblages with high-performance dry connections. *Engineering Structures* 2019;198:109552.
- 499 [16] Qian K, Liang SL, Xiong XY, Fu F, Fang Q. Quasi-static and dynamic behavior of precast concrete  
500 frames with high performance dry connections subjected to loss of a penultimate column scenario.  
501 *Engineering Structures* 2020;205:110115.
- 502 [17] Qian K, Liang SL, Feng DC, Fu F, Wu G. Experimental and Numerical Investigation on Progressive  
503 Collapse Resistance of Post-Tensioned Precast Concrete Beam-Column Subassemblages. *Journal of*  
504 *Structural Engineering* 2020;146(9):04020170.

- 505 [18] Karayannis CG, Goliás E. Full-scale experimental testing of RC beam-column joints strengthened  
506 using CFRP ropes as external reinforcement. *Engineering Structures* 2022;250:113305.
- 507 [19] Goliás E, Zapris AG, Kytinou VK, Kalogeropoulos GI, Chalioris CE, Karayannis CG. Effectiveness  
508 of the novel rehabilitation method of seismically damaged RC joints using C-FRP ropes and  
509 comparison with widely applied method using C-FRP sheets—Experimental investigation.  
510 *Sustainability* 2021;13(11):6454.
- 511 [20] Chalioris CE, Zapris AG, Karayannis CG. U-jacketing applications of fiber-reinforced polymers in  
512 reinforced concrete T-beams against shear—Tests and design. *Fibers* 2020;8(2):13.
- 513 [21] Kakaletsis DJ, David KN, Karayannis CG. Effectiveness of some conventional seismic retrofitting  
514 techniques for bare and infilled R/C frames. *Structural Engineering and Mechanics* 2011;39(4):499-  
515 520.
- 516 [22] Orton S, Jirsa JO, Bayrak O. Carbon fiber-reinforced polymer for continuity in existing reinforced  
517 concrete buildings vulnerable to collapse. *ACI Structural Journal* 2009;106(5):608-16.
- 518 [23] Kim I, Jirsa JO, Bayrak O. Use of carbon fiber-reinforced polymer to provide continuity in reinforced  
519 concrete beams under dynamic loading. *ACI Structural Journal* 2015;112(3):383-95.
- 520 [24] Qian K, Li B. Strengthening of multibay reinforced concrete flat slabs to mitigate progressive  
521 collapse. *Journal of Structural Engineering* 2015;141(6):04014154.
- 522 [25] Liu T, Xiao Y, Yang J, Chen BS. CFRP strip cable retrofit of RC frame for collapse resistance.  
523 *Journal of Composites for Construction* 2017;21(1):04016067.
- 524 [26] Feng P, Qiang H, Ou X, Qin W, Yang J. Progressive collapse resistance of GFRP-strengthened RC  
525 beam–slab subassemblages in a corner column–removal scenario. *Journal of Composites for*  
526 *Construction* 2019;23(1):04018076.
- 527 [27] Elsanadedy HM, Al-Salloum YA, Alrubaidi MA, Almusallam TH, Siddiqui NA, Abbas H.  
528 Upgrading of precast RC beam-column joints using innovative FRP/steel hybrid technique for  
529 progressive collapse prevention. *Construction and Building Materials* 2021;268:121130.
- 530 [28] ACI (American Concrete Institute). Building code requirements for structural concrete and  
531 commentary. ACI 318-19. Farmington Hills, MI: ACI. 2019.

- 532 [29] ACI (American Concrete Institute). Guide for the design and construction of externally bonded FRP  
533 systems for strengthening concrete structures. ACI 4402R-17. Farmington Hills, Michigan, ACI  
534 Committee 440. 2017.
- 535 [30] Izzuddin BA, Vlassis AG, Elghazouli AY, Nethercot DA. Progressive collapse of multi-storey  
536 buildings due to sudden column loss—Part I: Simplified assessment framework. *Engineering*  
537 *Structures* 2008;30(5):1308-18.
- 538 [31] DoD (US Department of Defense). Design of buildings to resist progressive collapse: unified  
539 facilities criteria ( UFC) 4-023-03. Washington DC, US Department of Defense ( DoD). 2016.
- 540 [32] GSA (US General Services Administration). Progressive collapse analysis and design guidelines for  
541 New Federal Office Buildings and major modernization projects. Washington DC, US General  
542 Services Administration. 2016.
- 543 [33] MOHURD (Ministry of Housing and Urban-Rural Development of the People's Republic of China).  
544 Code for design of concrete structures. GB 50010-15. Beijing: China, Architecture & Building Press.  
545 2015.
- 546 [34] Yu J, Tan KH. Special detailing techniques to improve structural resistance against progressive  
547 collapse. *Journal of Structural Engineering* 2014;140(3):04013077.
- 548 [35] Kang SB, Tan KH. Behaviour of precast concrete beam–column sub-assemblages subject to column  
549 removal. *Engineering Structures* 2015;93:85-96.
- 550 [36] Kang SB, Tan KH, Yang EH. Progressive collapse resistance of precast beam–column sub-  
551 assemblages with engineered cementitious composites. *Engineering Structures* 2015;98:186-200.
- 552 [37] Qian K, Li B, Ma JX. Load-carrying mechanism to resist progressive collapse of RC buildings.  
553 *Journal of Structural Engineering* 2015;141(2):04014107.
- 554 [38] Alogla K, Weekes L, Augustus-Nelson L. A new mitigation scheme to resist progressive collapse  
555 of RC structures. *Construction and Building Materials* 2016;125:533-45.
- 556 [39] Ren P, Li Y, Lu X, Guan H, Zhou Y. Experimental investigation of progressive collapse resistance  
557 of one-way reinforced concrete beam–slab substructures under a middle-column-removal scenario.  
558 *Engineering Structures* 2016;118:28-40.
- 559 [40] Lim NS, Tan KH, Lee CK. Experimental studies of 3D RC substructures under exterior and corner  
560 column removal scenarios. *Engineering Structures* 2017;150:409-27.

- 561 [41] Lim NS, Tan KH, Lee CK. Effects of rotational capacity and horizontal restraint on development of  
562 catenary action in 2-D RC frames. *Engineering Structures* 2017;153:613-27.
- 563 [42] Diao MZ, Li Y, Guan H, Lu XZ, Gilbert BP. Influence of horizontal restraints on the behaviour of  
564 vertical disproportionate collapse of RC moment frames. *Engineering Failure Analysis*  
565 2020;109:104324.
- 566 [43] Feng FF, Hwang HJ, Yi WJ. Static and dynamic loading tests for precast concrete moment frames  
567 under progressive collapse. *Engineering Structures* 2020;213.
- 568 [44] Zhang WX, Wu H, Zhang JY, Hwang HJ, Yi WJ. Progressive collapse test of assembled monolithic  
569 concrete frame spatial substructures with different anchorage methods in the beam-column joint.  
570 *Advances in Structural Engineering* 2020;23(9):1-15.
- 571 [45] Gu XL, Zhang B, Wang Y, Wang XL. Experimental investigation and numerical simulation on  
572 progressive collapse resistance of RC frame structures considering beam flange effects. *Journal of*  
573 *Building Engineering* 2021;42:102797.
- 574 [46] Long X, Wang S, Huang X-J, Li C, Kang S-B. Progressive collapse resistance of exterior reinforced  
575 concrete frames and simplified method for catenary action. *Engineering Structures*  
576 2021;249:113316.
- 577 [47] Qian K, Liang SL, Fu F, Li Y. Progressive collapse resistance of emulative precast concrete frames  
578 with various reinforcing details. *Journal of Structural Engineering* 2021;147(8):04021107.
- 579 [48] Qian K, Geng SY, Liang SL, Fu F, Yu J. Effects of loading regimes on the structural behavior of RC  
580 beam-column sub-assemblages against disproportionate collapse. *Engineering Structures*  
581 2022;251:113470.
- 582 [49] Qian K, Lan DQ, Zhang L, Fu F, Fang Q. Robustness of post-tensioned concrete beam-column  
583 subassemblies under various column removal scenarios. *Journal of Structural Engineering*  
584 2022;148(5):04022032.
- 585 [50] Park R, Paulay T. CH4-Strength of Members with Flexure. *Reinforced concrete structures*. John  
586 Wiley & Sons; 2000.
- 587 [51] ASCE (American Society of Civil Engineers). *Seismic rehabilitation and retrofit of existing*  
588 *buildings*. ASCE-41 17 Reston, VA, ASCE-41 17. 2017.

- 589 [52] Liang SL, Li Z, Wang CL, Qian K. Experimental and analytical study on the compressive arch action  
590 of precast concrete assemblies with monolithic connections to resist progressive collapse. Journal of  
591 Structural Engineering 2023;149(4):04023010.
- 592 [53] Yu J, Tan KH. Analytical model for the capacity of compressive arch action of reinforced concrete  
593 sub-assemblages. Magazine of Concrete Research 2014;66(3):109-26.
- 594 [54] Yu J, Yin C, Guo Y. Nonlinear SDOF model for progressive collapse responses of structures with  
595 consideration of viscous damping. Journal of Engineering Mechanics 2017;143(9):04017108.
- 596
- 597

598

599

**Table 1** Details of the sub-frames

Sub-frame	Element size b×h (mm×mm)		Beam reinforcement				Location of the removed column	Strengthened load transfer mechanism
	Beam	Column	Ends		Middle			
			Top	Bottom	Top	Bottom		
P-R							Penultimate	N/A
E-R							Edge	N/A
P-S-C							Penultimate	CAA
P-S-CC	150×250	250×250	3T10	2T10	2T10	2T10	Penultimate	CAA and CA
E-S-C							Edge	CA
E-S-CC1							Edge	CAA and CA
E-S-CC2							Edge	CAA and CA

600

601

602

**Table 2** Material properties of the reinforcement and CFRP

Rebar	Nominal diameter (mm)	Yield strength (MPa)	Ultimate strength (MPa)	Elongation (%)
	T12	12	462	596
T10	10	532	663	12.8
R6	6	368	485	21.0
CFRP	Thickness (mm)	Elastic modulus (MPa)	Ultimate strength (MPa)	Elongation (%)
	0.167	3,467	241,000	1.71

603

604

605

**Table 3** Critical test results

Sub-frame	Critical load resistance capacity (kN)			Critical displacements (mm)			L/RMHCRF (kN)	L/RMHTRF (kN)
	YL	CAA	CA	YL	CAA	CA		
P-R	33	42	33	30	70	552	-76/-61	90/73
E-R	35	45	40	20	73	532	-82	102
P-S-C	40	49	24	15	55	560	-91/-78	67/58
P-S-CC	44	52	55	25	64	621	-98/-85	125/113
E-S-C	36	47	46	25	100	567	-87	111
E-S-CC1	47	58	58	25	110	597	-111	138
E-S-CC2	42	53	49	23	60	577	-101	119

606

607

**Table 4** Database for comparison of the acceptable plastic rotations for collapse prevention with the measured ones

Papers	Specimen ID	Beam clear span (mm)	Critical beam section			$(\rho - \rho')$ $\rho_{bal}$	Beam type	Critical displacement (mm)		Measured plastic rotation (rad)		$[\theta]$ (rad)		$\theta_{CAA}/[\theta]$	
			b×h (mm×mm)	$\rho$ (%)	$\rho'$ (%)			$d_y$	$d_{CAA}$	$\theta_y$	$\theta_{CAA}$	DoD	GSA	DoD	GSA
This study	P-R	2,750	150×250	0.47	0.70	$\leq 0$	NC	30	70	0.0109	0.0145	0.05	0.06	0.29	0.24
	E-R	2,750	150×250	0.47	0.70		NC	20	73	0.0073	0.0193	0.05	0.06	0.39	0.32
Su et al. [2]	A1	1,225	150×300	0.55	0.55	$\leq 0$	NC	/	48.0	/	0.0392	0.05	0.06	0.78	0.65
	A2	1,225	150×300	0.83	0.83		C	/	56.4	/	0.0460	0.063	0.1	0.73	0.46
	A3	1,225	150×300	1.13	1.13		C	/	76.4	/	0.0624	0.063	0.1	0.99	0.62
	A4	1,225	150×300	0.38	0.55		NC	/	65.0	/	0.0531	0.05	0.06	1.06	0.89
	A5	1,225	150×300	0.55	0.83		C	/	70.7	/	0.0577	0.063	0.1	0.92	0.58
	A6	1,225	150×300	0.75	1.13		C	/	69.2	/	0.0565	0.063	0.1	0.90	0.57
	B1	1,975	150×300	1.13	1.13		NC	/	100.0	/	0.0506	0.05	0.06	1.01	0.84
	B2	2,725	150×300	1.13	1.13		NC	/	102.0	/	0.0374	0.05	0.06	0.75	0.62
	B3	2,725	150×300	0.75	1.13		NC	/	85.5	/	0.0314	0.05	0.06	0.63	0.52
	C1	1,225	150×200	1.30	1.30		NC	/	33.7	/	0.0275	0.05	0.06	0.55	0.46
Choi and Kim [3]	5G	1,510	185×150	0.66	0.66	$\leq 0$	NC	/	84.5	/	0.0560	0.05	0.06	1.12	0.93
	5S	1,505	150×225	0.53	1.31		C	/	103.0	/	0.0684	0.063	0.1	1.09	0.68
	8G	1,510	125×160	0.94	0.94		NC	/	59.0	/	0.0391	0.05	0.06	0.78	0.65
	8S	1,505	140×195	1.00	1.66		C	/	59.3	/	0.0394	0.063	0.1	0.63	0.39
Sadek et al. [4]	IMF	5,385	711×508	0.40	0.63	$\leq 0$	C	/	127	/	0.0236	0.063	0.1	0.37	0.24
	SMF	5,233	864×660	0.59	0.69		C	/	112	/	0.0214	0.063	0.1	0.34	0.21
FarhangVesali et al. [5]	1	2,110	180×180	0.59	0.59	$\leq 0$	NC	/	49.0	/	0.0232	0.05	0.06	0.46	0.39
	2	2,110	180×180	0.59	0.59		NC	/	44.0	/	0.0209	0.05	0.06	0.42	0.35
	3	2,110	180×180	0.59	0.59		NC	/	50.0	/	0.0237	0.05	0.06	0.47	0.40
	4	2,110	180×180	0.59	0.88		NC	/	54.0	/	0.0256	0.05	0.06	0.51	0.43
	5	2,110	180×180	0.59	0.88		NC	/	54.0	/	0.0256	0.05	0.06	0.51	0.43
	6	2,110	180×180	0.59	0.88		NC	/	52.0	/	0.0246	0.05	0.06	0.49	0.41
Qian and Li [9]	F1	2,175	100×180	0.87	0.87	$\leq 0$	NC	13.5	15.4	0.0062	0.0071	0.05	0.06	0.14	0.12
	F2	2,175	100×180	1.47	1.47		NC	15.2	21.3	0.0070	0.0098	0.05	0.06	0.20	0.16
	F3	2,175	100×180	0.87	0.87		NC	7.2	30.0	0.0033	0.0138	0.05	0.06	0.28	0.23
	F4	2,175	100×180	0.87	0.87		NC	16.3	17.8	0.0075	0.0082	0.05	0.06	0.16	0.14
	F5	2,775	240×100	0.65	0.65		NC	20.0	26.1	0.0072	0.0094	0.05	0.06	0.19	0.16
	F6	2,175	100×180	0.87	0.65		NC	17.2	23.5	0.0079	0.0108	0.05	0.06	0.22	0.18
	F7	2,175	100×180	0.87	0.75		NC	13.3	20.2	0.0061	0.0093	0.05	0.06	0.19	0.16
Yu and Tan	S1	2,750	150×250	0.49	0.90	$\leq 0$	NC	/	78.0	/	0.0284	0.05	0.06	0.57	0.47

[7]	S2	2,750	150×250	0.49	0.73		NC	/	73.0	/	0.0265	0.05	0.06	0.53	0.44
	S3	2,750	150×250	0.49	1.24		NC	/	74.4	/	0.0271	0.05	0.06	0.54	0.45
	S4	2,750	150×250	0.82	1.24		NC	/	81.0	/	0.0295	0.05	0.06	0.59	0.49
	S5	2,750	150×250	1.24	1.24		NC	/	74.5	/	0.0271	0.05	0.06	0.54	0.45
	S6	2,750	150×250	0.82	1.87		NC	/	114.4	/	0.0416	0.05	0.06	0.83	0.69
	S7	2,150	150×250	0.82	1.24		NC	/	74.4	/	0.0346	0.05	0.06	0.69	0.58
	S8	1,550	150×250	0.82	1.24		NC	/	45.9	/	0.0296	0.05	0.06	0.59	0.49
	Yu and Tan [34]	F1-CD	2,750	150×250	0.82		1.24	∇	NC	/	61.4	/	0.0223	0.05	0.06
F2-MR		2,750	150×250	0.82	1.24	NC	/		87.0	/	0.0316	0.05	0.06	0.63	0.53
F3-PD		2,750	150×250	0.82	1.24	NC	/		77.4	/	0.0281	0.05	0.06	0.56	0.47
F4-PH		2,750	150×250	0.90	1.24	NC	/		94.8	/	0.0345	0.05	0.06	0.69	0.58
Kang and Tan [35]	MJ-B-0.52/0.35S	2,750	150×300	0.35	0.52	∇	C	/	76.7	/	0.0279	0.063	0.1	0.44	0.28
	MJ-L-0.52/0.35S	2,750	150×300	0.35	0.52		C	/	71.8	/	0.0261	0.063	0.1	0.41	0.26
	MJ-B-0.88/0.59R	2,750	150×300	0.59	0.88		C	/	100.9	/	0.0367	0.063	0.1	0.58	0.37
	MJ-L-0.88/0.59R	2,750	150×300	0.59	0.88		C	/	100.9	/	0.0367	0.063	0.1	0.58	0.37
	MJ-L-1.19/0.59R	2,750	150×300	0.59	1.19		C	/	105.7	/	0.0384	0.063	0.1	0.61	0.38
Kang et al. [36]	EMJ-B-1.19/0.59	2,750	150×300	0.59	1.19	∇	C	/	108.9	/	0.0396	0.063	0.1	0.63	0.40
	EMJ-L-1.19/0.59	2,750	150×300	0.59	1.19		C	/	103.1	/	0.0375	0.063	0.1	0.60	0.38
	EMJ-B-0.88/0.59	2,750	150×300	0.59	0.88		C	/	101.9	/	0.0371	0.063	0.1	0.59	0.37
	EMJ-L-0.88/0.59	2,750	150×300	0.59	0.88		C	/	106.9	/	0.0389	0.063	0.1	0.62	0.39
	EMJ-L-0.88/0.88	2,750	150×300	0.88	0.88		C	/	171.2	/	0.0623	0.063	0.1	0.99	0.62
Qian et al. [37]	P1	1,300	100×180	0.87	0.87	∇	NC	16.8	37.3	0.0129	0.0158	0.05	0.06	0.32	0.26
	P2	1,300	80×140	1.40	1.40		NC	14.1	30.8	0.0108	0.0128	0.05	0.06	0.26	0.21
Vali pour et al. [10]	No. 1	2,110	180×180	0.59	0.87	∇	NC	/	59.0	/	0.0260	0.05	0.06	0.52	0.43
	No. 2	2,110	180×180	0.59	0.59		NC	/	54.8	/	0.0260	0.05	0.06	0.52	0.43
	No. 3	2,110	180×180	0.59	0.87		NC	/	55.4	/	0.0263	0.05	0.06	0.53	0.44
	No. 4	2,110	180×180	0.59	0.59		NC	/	56.3	/	0.0267	0.05	0.06	0.53	0.45
Alogla et al. [38]	SS-1	2,775	150×250	0.48	0.72	∇	NC	57.9	101.0	0.0209	0.0155	0.05	0.06	0.31	0.26
	SS-2	2,775	150×250	0.48	0.72		NC	55.1	96.8	0.0199	0.0150	0.05	0.06	0.30	0.25
	SS-3	2,775	150×250	0.48	0.72		NC	48.2	86.8	0.0174	0.0139	0.05	0.06	0.28	0.23
	SS-4	2,775	150×250	0.48	0.72		NC	60.1	91.4	0.0217	0.0113	0.05	0.06	0.23	0.19
Kang and Tan [12]	EF-B	2,750	150×300	0.59	1.19	∇	C	/	111.2	/	0.0404	0.063	0.1	0.64	0.40
	EF-L	2,750	150×300	0.59	1.19		C	/	72.1	/	0.0262	0.063	0.1	0.42	0.26
	EF-B-S	2,700	150×300	0.59	1.19		C	/	87.2	/	0.0323	0.063	0.1	0.51	0.32
	EF-L-S	2,700	150×300	0.59	1.19		C	/	78.2	/	0.0290	0.063	0.1	0.46	0.29
Ren et al. [39]	B2	1,900	85×170	0.81	1.04	∇	NC	/	33.0	/	0.0174	0.05	0.06	0.35	0.29
	B3	1,900	85×200	0.70	0.92		NC	/	33.3	/	0.0175	0.05	0.06	0.35	0.29
Lim et al.	COR	2,220	100×180	1.02	1.53	∇	NC	/	108	/	0.0486	0.05	0.06	0.97	0.81

[40]	EXT	2,220	100×180	1.02	1.53		NC	/	108	/	0.0486	0.05	0.06	0.97	0.81
Lim et al. [41]	FR	2,400	100×180	1.01	1.52	∇0	NC	46	84	0.0192	0.0158	0.05	0.06	0.32	0.26
	FR-S	2,400	100×180	1.01	1.52		C	45	95	0.0188	0.0208	0.063	0.1	0.33	0.21
	FR-R	2,400	100×180	1.33	2.02		C	34	70	0.0142	0.0150	0.063	0.1	0.24	0.15
	IR-1	2,400	100×180	1.01	1.52		NC	46	89	0.0192	0.0179	0.05	0.06	0.36	0.30
	IR-2	2,400	100×180	1.01	1.52		NC	53	70	0.0221	0.0071	0.05	0.06	0.14	0.12
Yu and Tan [13]	F2-WS	2,750	150×250	0.82	1.24	∇0	NC	/	84.8	/	0.0308	0.05	0.06	0.62	0.51
	F3-NS-H	2,750	150×250	0.82	1.24		NC	/	84.4	/	0.0307	0.05	0.06	0.61	0.51
	F4-WS-H	2,750	150×250	0.82	1.24		NC	/	84.4	/	0.0307	0.05	0.06	0.61	0.51
Deng et al. [11]	NSC-8	2,000	150×250	0.67	1.01	∇0	NC	25	79	0.0125	0.0270	0.05	0.06	0.54	0.45
	NSC-11	2,750	150×250	0.67	1.01		NC	36	90	0.0131	0.0196	0.05	0.06	0.39	0.33
	NSC-13	3,250	150×250	0.67	1.01		NC	45	108	0.0138	0.0194	0.05	0.06	0.39	0.32
	HSC-8	2,000	150×250	0.67	1.01		NC	16	80	0.0080	0.0320	0.05	0.06	0.64	0.53
	HSC-11	2,750	150×250	0.67	1.01		NC	28	74	0.0102	0.0167	0.05	0.06	0.33	0.28
	HSC-13	3,250	150×250	0.67	1.01		NC	35	104	0.0108	0.0212	0.05	0.06	0.42	0.35
Diao et al. [42]	OP	2,250	100×250	0.70	0.70	∇0	NC	18	65	0.0080	0.0209	0.05	0.06	0.42	0.35
	OA	2,250	100×250	0.70	0.70		NC	15	50	0.0067	0.0156	0.05	0.06	0.31	0.26
	TP	2,250	100×250	0.70	0.70		NC	15	91	0.0067	0.0338	0.05	0.06	0.68	0.56
Feng et al. [43]	PCF-1	2,600	150×250	0.69	1.24	∇0	C	/	79.2	/	0.0305	0.063	0.1	0.48	0.31
	PCF-2	2,600	180×300	0.37	0.65		C	/	79.2	/	0.0305	0.063	0.1	0.48	0.31
	PCF-3	2,600	180×300	0.37	0.65		C	/	93.4	/	0.0359	0.063	0.1	0.57	0.36
	PCF-4	2,600	150×250	0.69	1.24		C	/	86.2	/	0.0332	0.063	0.1	0.53	0.33
Zhang et al. [44]	PC-H	3,600	200×420	0.50	0.75	∇0	C	18.1	86.0	0.0050	0.0189	0.063	0.1	0.30	0.19
	PC-L	3,600	200×420	0.64	0.75		C	41.6	81.6	0.0116	0.0111	0.063	0.1	0.18	0.11
	PC-A	3,600	200×420	0.50	0.75		C	20.6	90.2	0.0057	0.0193	0.063	0.1	0.31	0.19
Gu et al. [45]	B1A	1,800	100×150	0.80	0.80	∇0	NC	39.6	50.9	0.0220	0.0063	0.05	0.06	0.13	0.11
	B1	1,800	100×150	0.80	0.80		NC	26.7	63.9	0.0148	0.0207	0.05	0.06	0.41	0.35
	TB3	1,800	100×150	0.80	0.80		NC	12.9	64.2	0.0072	0.0285	0.05	0.06	0.57	0.48
	TB4	1,800	100×150	0.80	0.80		NC	13.3	70.5	0.0074	0.0318	0.05	0.06	0.64	0.53
	TB5	1,800	100×150	0.80	0.80		NC	27.1	56.5	0.0151	0.0163	0.05	0.06	0.33	0.27
Long et al. [46]	FN-1.05	2,450	150×250	0.67	1.01	∇0	NC	/	80	/	0.0327	0.05	0.06	0.65	0.55
	FS-1.05	2,450	150×250	0.67	1.01		C	/	102	/	0.0416	0.063	0.1	0.66	0.42
	FS-1.43	2,450	150×250	0.67	1.37		C	/	95	/	0.0388	0.063	0.1	0.62	0.39
	FS-1.43E	2,450	150×250	0.67	1.37		C	/	76	/	0.0310	0.063	0.1	0.49	0.31
	FS-1.86E	2,450	150×250	0.67	1.79		C	/	68	/	0.0278	0.063	0.1	0.44	0.28
Qian et al. [47]	IA	2,750	150×250	0.67	1.01	∇0	NC	46	68	0.0167	0.0080	0.05	0.06	0.16	0.13
	SA	2,750	150×250	0.67	1.01		NC	31	66	0.0113	0.0127	0.05	0.06	0.25	0.21
	UB	2,750	150×250	0.67	1.01		NC	36	76	0.0131	0.0145	0.05	0.06	0.29	0.24

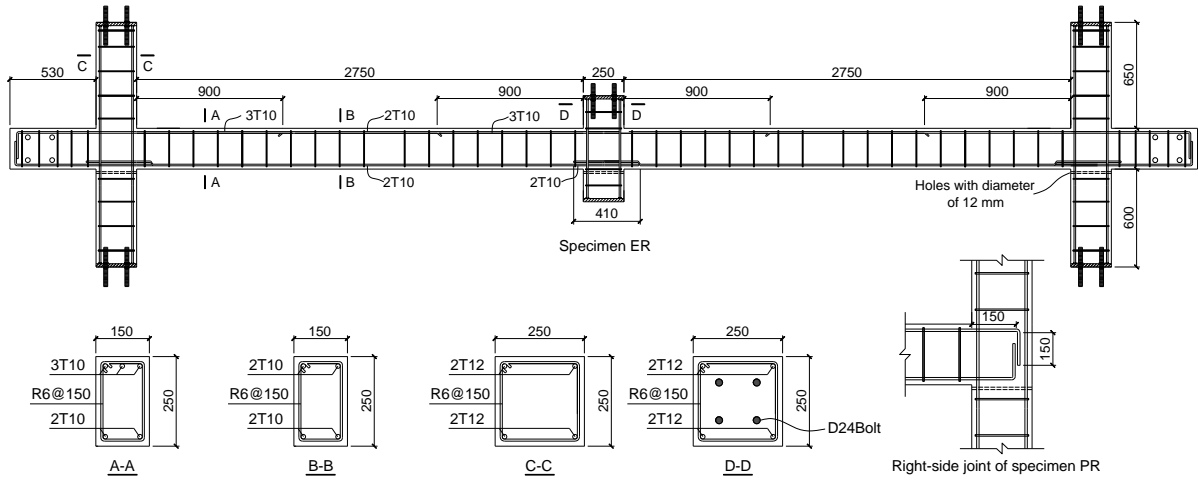
Qian et al. [48]	SL-8	2,000	150×250	0.67	1.01	0.119	NC	23	80	0.0115	0.0285	0.044	0.053	0.65	0.54
	SL-11	2,750	150×250	0.67	1.01	0.119	NC	35	90	0.0127	0.0200	0.044	0.053	0.45	0.38
	SL-13	3,250	150×250	0.67	1.01	0.119	NC	43	100	0.0132	0.0175	0.044	0.053	0.40	0.33
Qian et al. [49]	RCM	2,750	150×250	0.67	1.01	≤0	NC	30	70	0.0109	0.0145	0.05	0.06	0.29	0.24
	RCP	2,750	150×250	0.67	1.01		NC	27	76	0.0098	0.0178	0.05	0.06	0.36	0.30

609

610

611

612



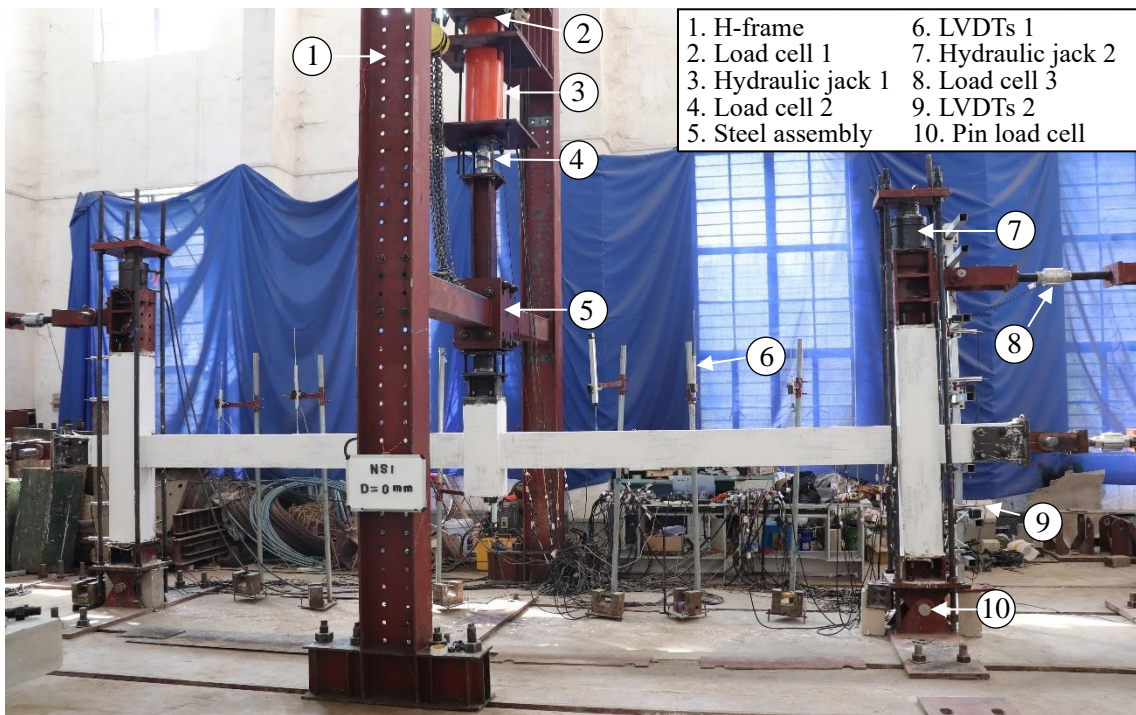
613

614

615

616

**Fig. 1** Geometric dimension and reinforcement arrangement of sub-frames

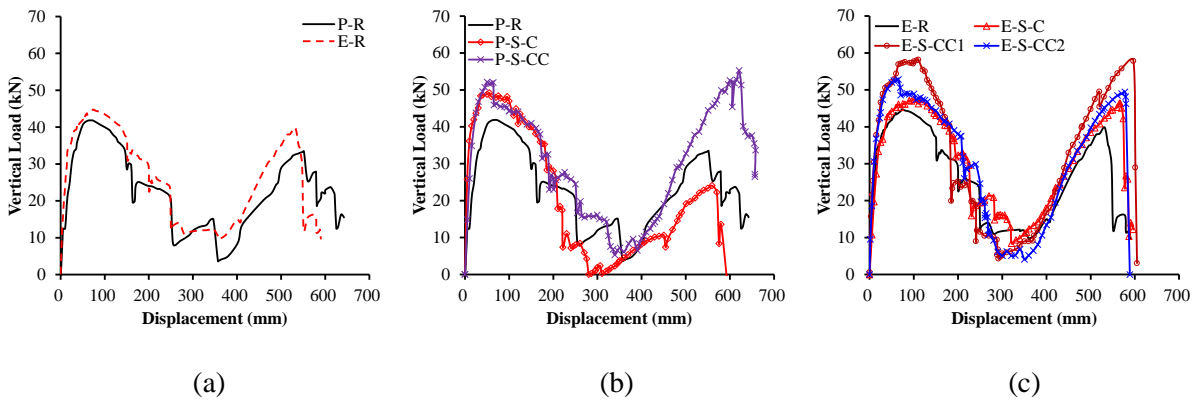


617

618

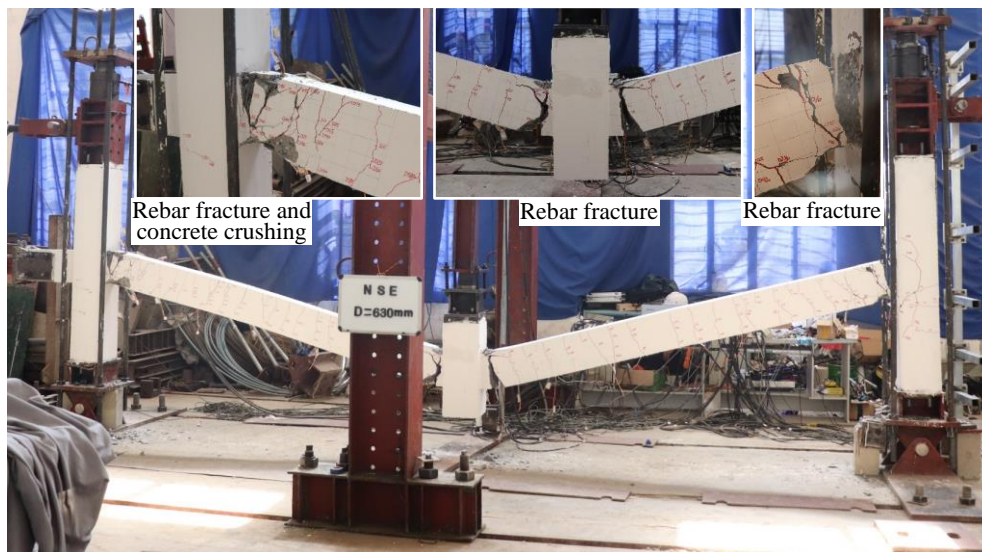
619

**Fig. 2** Test setup



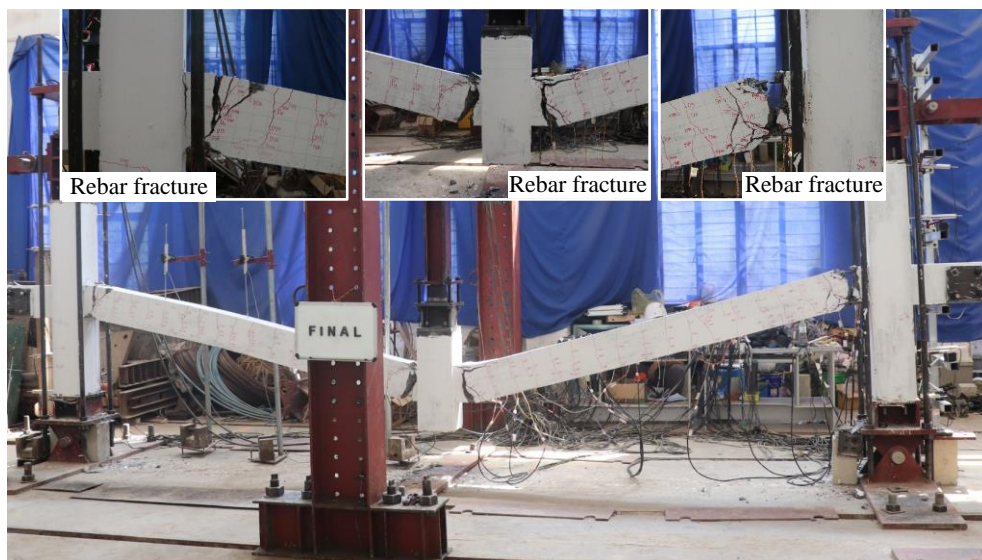
620  
621  
622  
623  
624

**Fig. 3** Load resistance-displacement history: (a) referential sub-frames; (b) P-series sub-frames; (c) E-series sub-frames



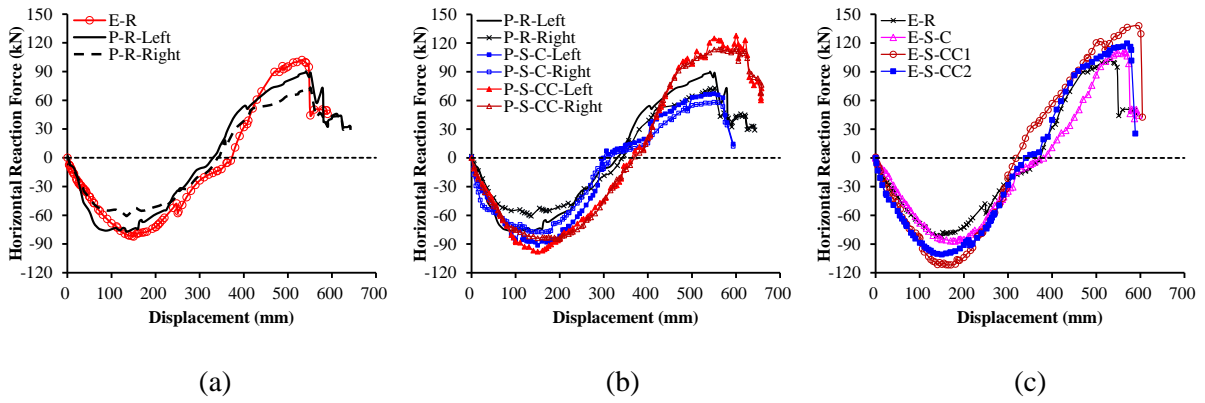
625  
626  
627

**Fig. 4** Failure mode of P-R

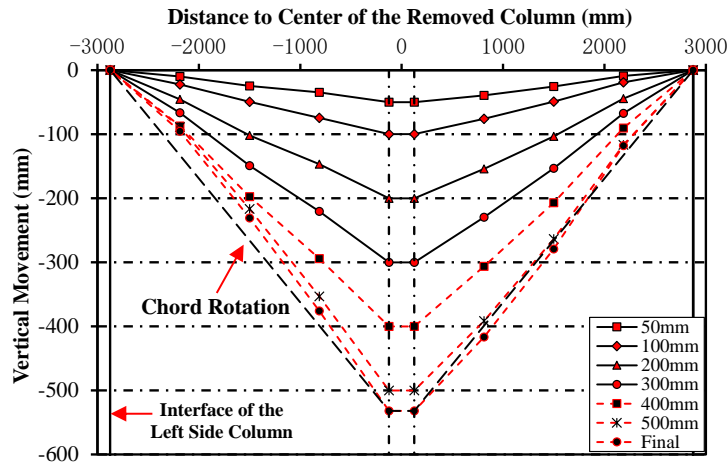


628  
629

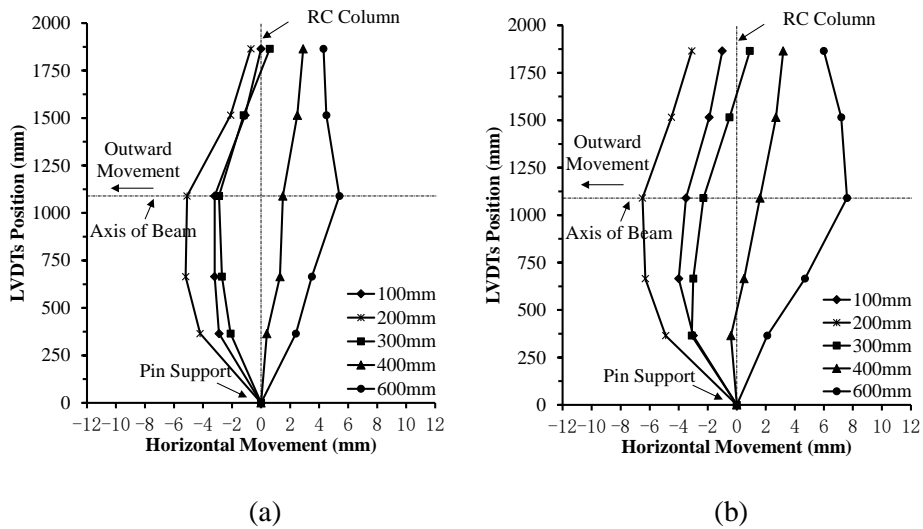
**Fig. 5** Failure mode of E-R



630  
631  
632 **Fig. 6** Horizontal reaction force-displacement history: (a) referential sub-frames; (b) P-series sub-frames; (c) E-series sub-frames

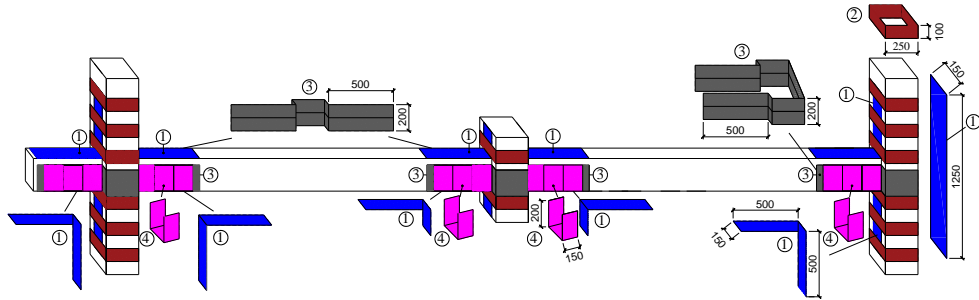


635  
636 **Fig. 7** Beam deflection of E-R



637  
638  
639 **Fig. 8** Deflection of the right side column: (a) E-R; (b) P-R

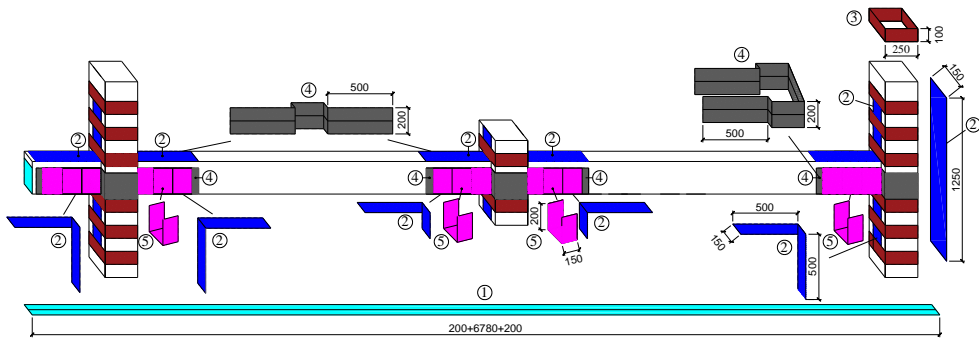
642



643

644

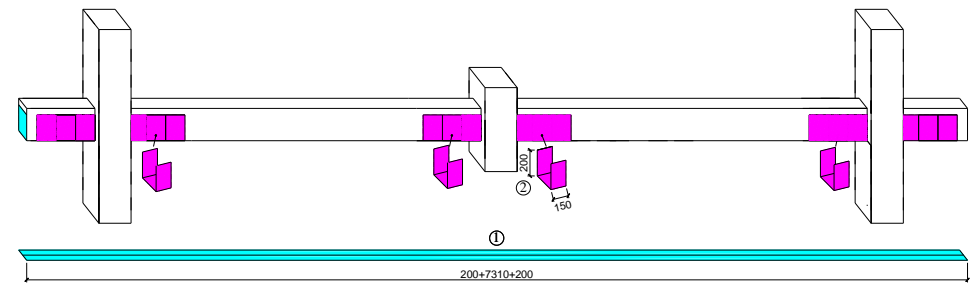
(a)



645

646

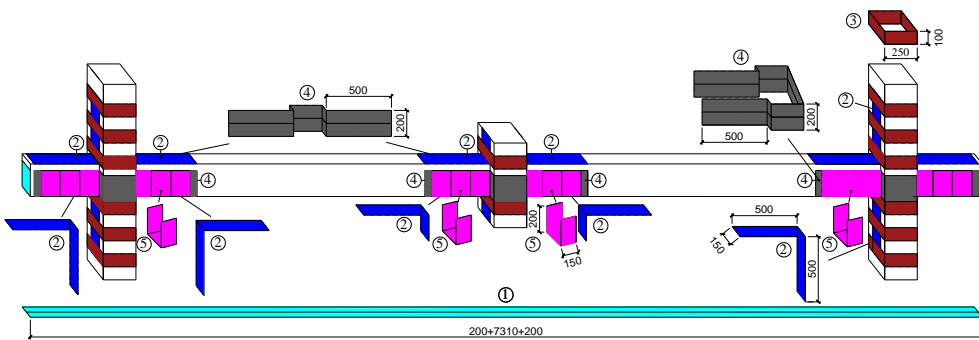
(b)



647

648

(c)



649

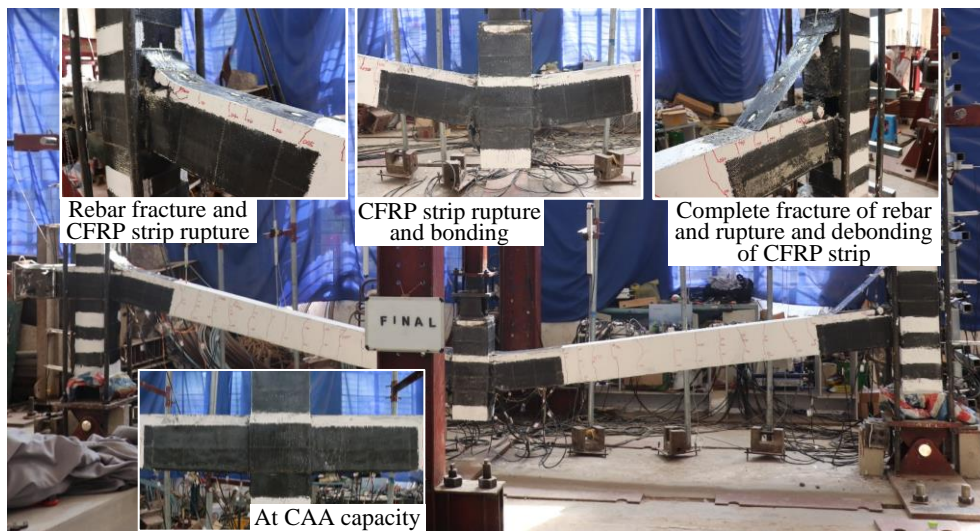
650

(d)

651 **Fig. 9** Strengthening scheme of sub-frames: (a) P-S-C; (b) P-S-CC; (c) E-S-C; (d) E-S-CC1 & E-S-CC2

652

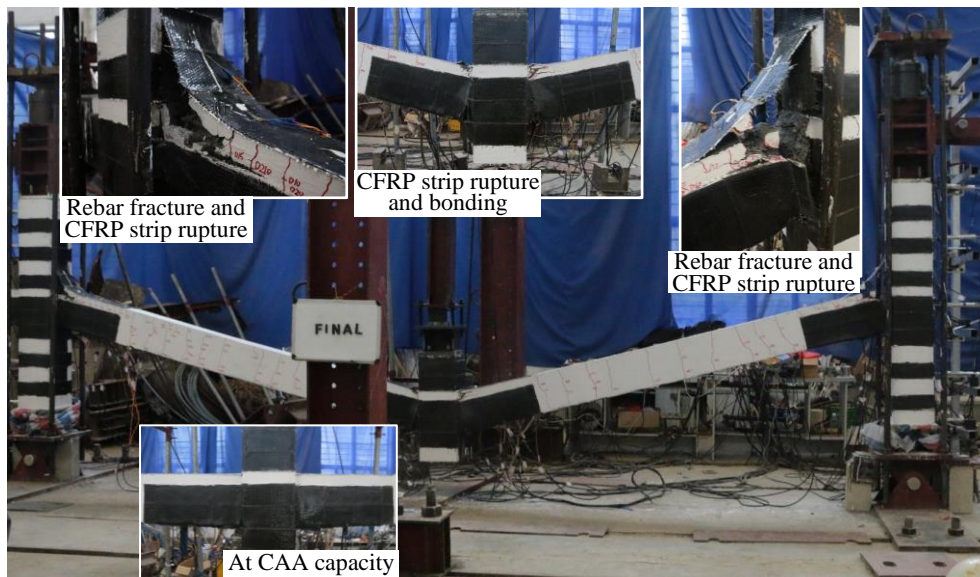
653



654

655

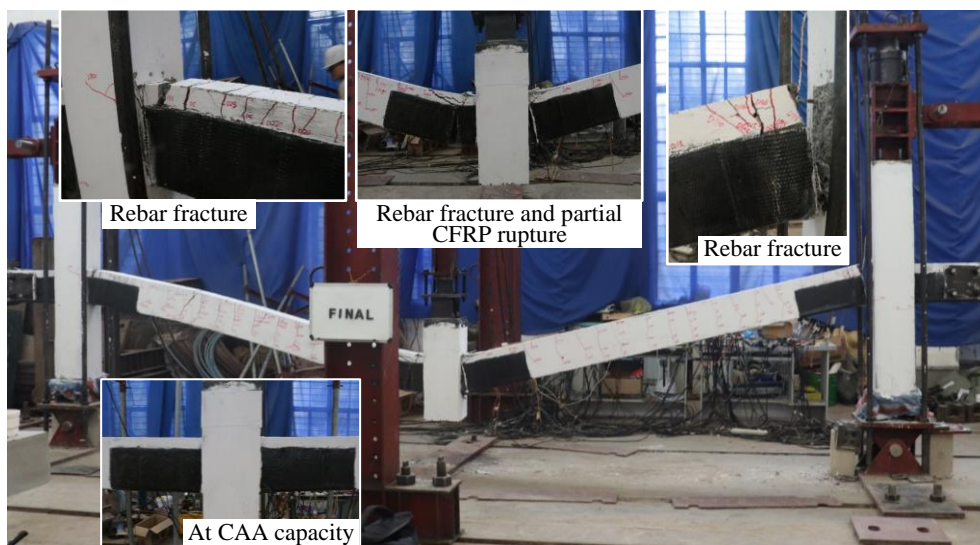
**Fig. 10** Failure mode of P-S-C



656

657

**Fig. 11** Failure mode of P-S-CC

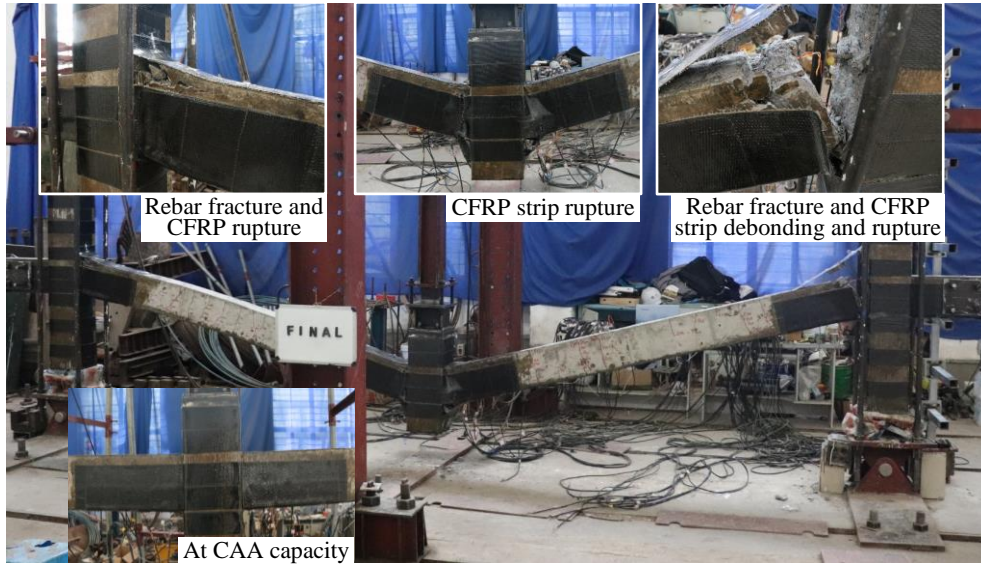


658

659

**Fig. 12** Failure mode of E-S-C

660

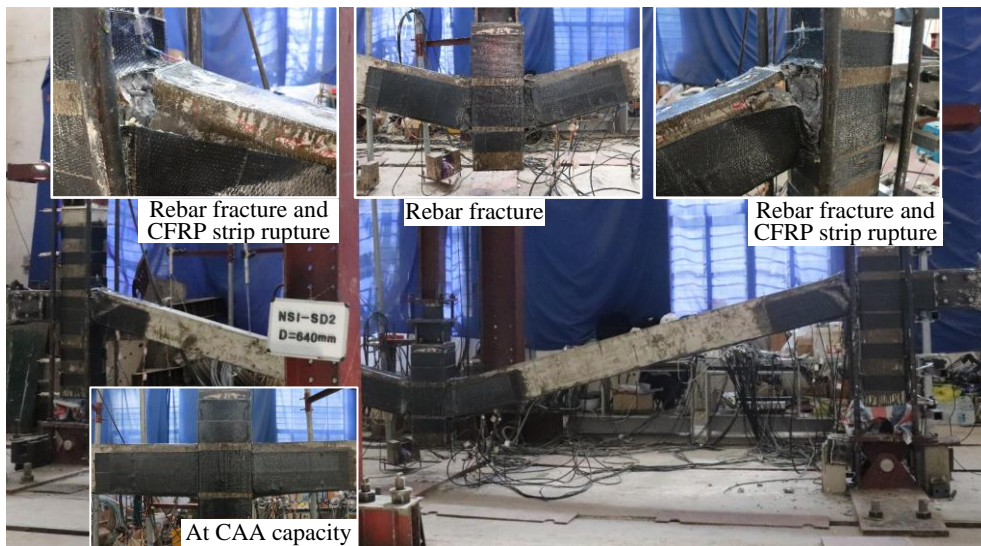


661

662

**Fig. 13** Failure mode of E-S-CC1

663



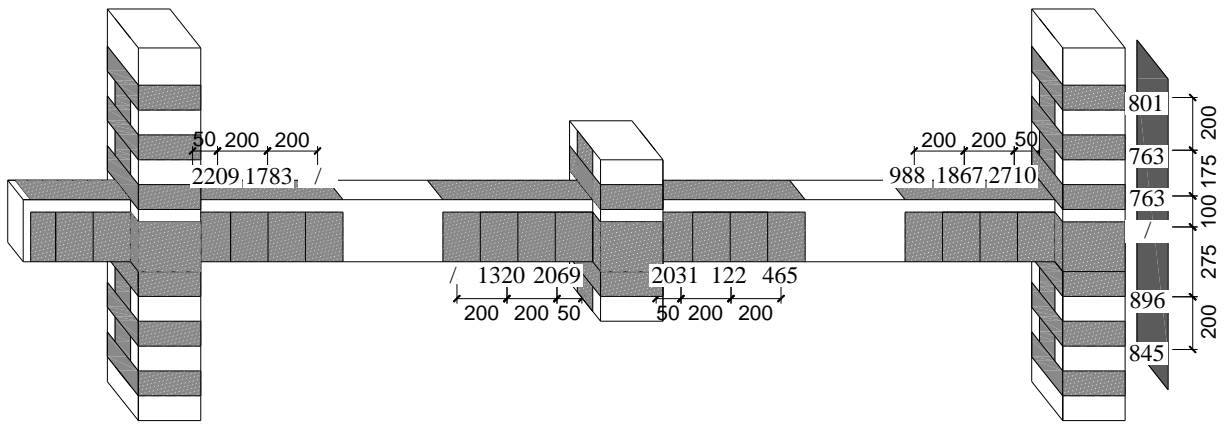
664

665

**Fig. 14** Failure mode of E-S-CC2

666

667



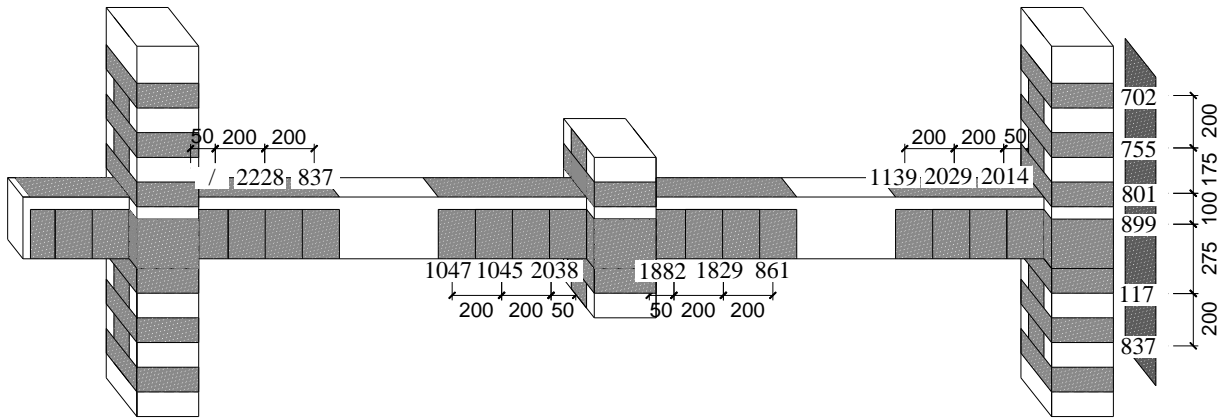
668

669

670

671

(a)



672

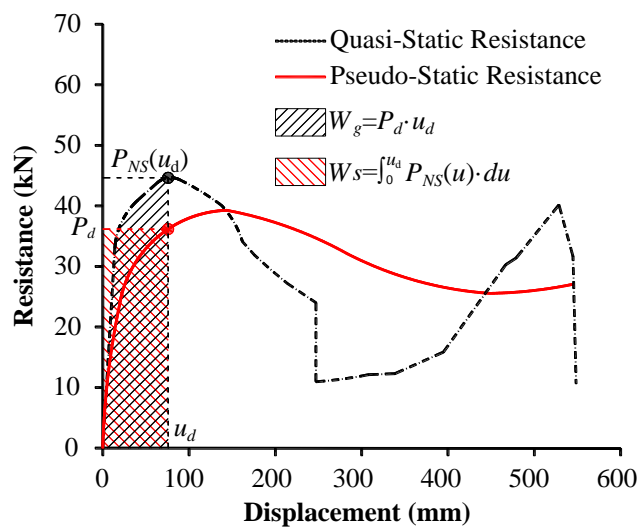
673

674

(b)

**Fig. 15** Strain of CFRP strips at CAA capacity: (a) P-S-C; (b) P-S-CC (unit in  $\mu\epsilon$ )

675

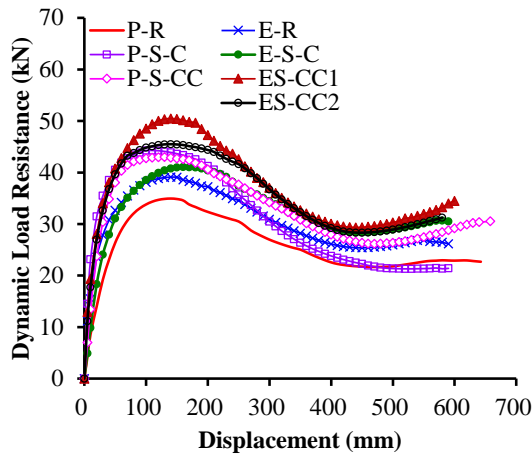


676

677

678

**Fig. 16** Illustration of the energy-based method

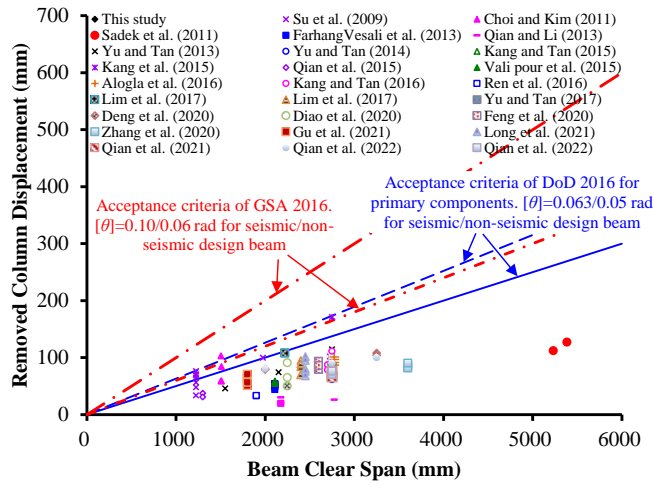


679

680

**Fig. 17** Dynamic collapse-resistant capacity of the sub-frames

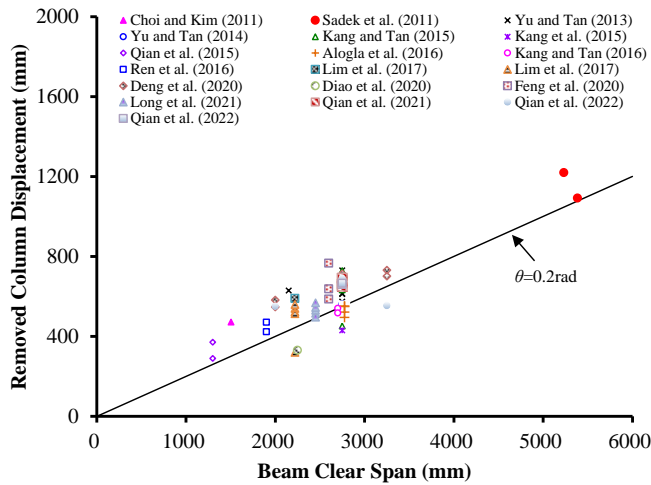
681



682

**Fig. 18** Comparison of the measured plastic rotations at CAA capacity with the acceptable ones

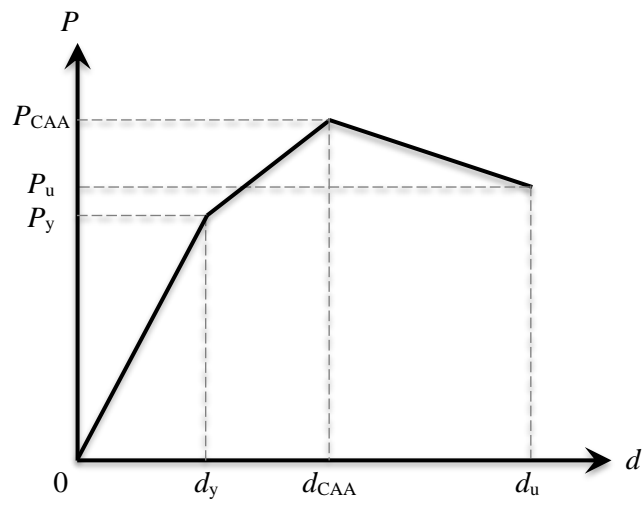
684



685

**Fig. 19** Measured plastic rotations at CA capacity for the beams with considerable CA capacities

687



688

689

690

691

**Fig. 20** Proposed load resistance function